NeuroImage 202 (2019) 116092

Contents lists available at ScienceDirect

NeuroImage

journal homepage: www.elsevier.com/locate/neuroimage

A putative human homologue of the macaque area PEc

Sabrina Pitzalis [a,b,*,1], Chiara Serra [a,b,1], Valentina Sulpizio [b,c], Sara Di Marco [a,b], Patrizia Fattori [c], Gaspare Galati [b,d], Claudio Galletti [c]

[a] Department of Movement, Human and Health Sciences, University of Rome "Foro Italico", 00135, Rome, Italy
[b] Department of Cognitive and Motor Rehabilitation and Neuroimaging, Santa Lucia Foundation (IRCCS Fondazione Santa Lucia), 00142, Rome, Italy
[c] Department of Biomedical and Neuromotor Sciences, University of Bologna, 40126, Bologna, Italy
[d] Brain Imaging Laboratory, Department of Psychology, Sapienza University, 00185, Rome, Italy

ARTICLE INFO

Keywords:
Superior parietal lobule
Optic flow
Pointing
Locomotion
Functional connectivity
Leg representation

ABSTRACT

The cortical area PEc is anatomically and functionally well-defined in macaque, but it is unknown whether it has a counterpart in human. Since we know that macaque PEc, but not the nearby posterior regions, hosts a lower limb representation, in an attempt to recognize a possible human PEc we looked for the existence of leg representations in the human parietal cortex using individual cortical surface-based analysis, task-evoked paradigms and resting-state functional connectivity. fMRI images were acquired while thirty-one participants performed long-range leg movements through an in-house MRI-compatible set-up. We revealed the existence of multiple leg representations in the human dorsomedial parietal cortex, here defined as S-I (somatosensory-I), hPE (human PE, in the post-central sulcus), and hPEc (human PEc, in the anterior precuneus). Among the three "leg" regions, hPEc had a unique functional profile, in that it was the only one responding to both arm and leg movements, to both hand-pointing and foot pointing movements, and to flow field visual stimulation, very similar to macaque area PEc. In addition, hPEc showed functional connections with the somatomotor regions hosting a lower limb representation, again as in macaque area PEc. Therefore, based on similarity in brain position, functional organization, cortical connections, and relationship with the neighboring areas, we propose that this cortical region is the human homologue of macaque area PEc.

1. Introduction

Classical models of sensorimotor integration describe the superior parietal lobule (SPL) as an associative cortical region at the interface between perception and action (Goodale and Milner, 1992; Astafiev et al., 2003). In monkey (Fig. 1A), the caudalmost part of SPL, i.e. the anterior bank of the parieto-occipital sulcus (POs), contains three cytoarchitectonically and functionally distinct areas: the visual motion area V6 (Galletti et al., 1996, 1999a; Luppino et al., 2005) and the two visuomotor areas V6Av and V6Ad (Galletti et al., 1999b; Luppino et al., 2005; Gamberini et al., 2011), both responding to arm reaching and grasping movements (Fattori et al., 2005, 2010). Moving anteriorly towards the tip of the cingulate sulcus (Cgs), the SPL encompasses two other regions which Pandya and Seltzer (1982), using the nomenclature proposed in humans by von Economo and Koskinas (1925), called PE, anteriorly, and PEc (where 'c' stands for caudal), posteriorly. Both regions show somatosensory and somatomotor responses and, unlike V6A, also represent the leg (Breveglieri et al., 2006; Taoka et al., 1998; Padberg et al., 2007; Seelke et al., 2012). The physiological and connectional properties suggest that PEc integrates motor and visual information and controls the interaction of the four limbs with the environment (Breveglieri et al., 2008; Bakola et al., 2010; Hadjidimitrakis et al., 2015; Gamberini et al., 2018; Impieri et al., 2018).

In human (Fig. 1B), the homologues of monkey areas V6 (Pitzalis et al., 2006), V6Av (Pitzalis et al., 2013d, 2015), and V6Ad (Tosoni et al., 2015) have been recently proposed based on their functional profile, topographical organization, and interhemispheric connections. In contrast, little is known about the existence of a human homologue of macaque area PEc. Many neuroimaging studies have reported that the dorsal precuneate cortex (where PEc should be located) responds to arm pointing and reaching/grasping movements like in macaque (e.g., Tosoni et al., 2008, 2015; Cavina-Pratesi et al., 2010; Filimon et al., 2007; Galati et al., 2011; Vesia et al., 2010; Magri et al., 2019). This long pointing-responsive strip of cortex (see cyan strip in Fig. 1B), which

* Corresponding author. Department of Movement, Human and Health Sciences, University of Rome "Foro Italico'', 00135, Rome, Italy.
E-mail address: sabrina.pitzalis@uniroma4.it (S. Pitzalis).
[1] Both authors contributed equally to this work.

https://doi.org/10.1016/j.neuroimage.2019.116092
Received 27 July 2019; Accepted 8 August 2019
Available online 10 August 2019

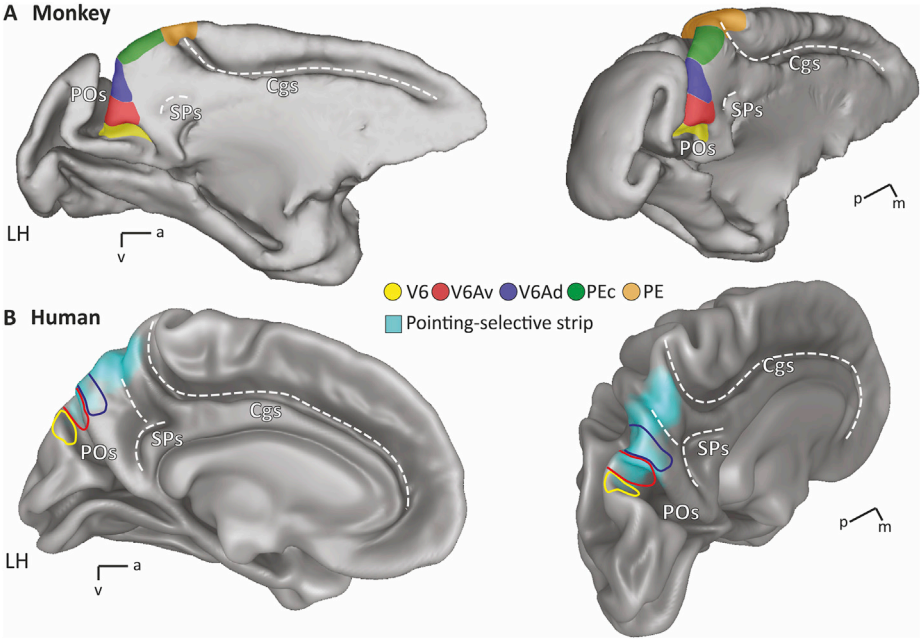

Fig. 1. Anatomy of the medial wall in monkey and human brains. (A) Medial (left) and dorsomedial (right) views of cortical surface reconstructions of a left macaque hemisphere (LH). The average extent and location of the cytoarchitectonically-defined areas are colour-outlined on each reconstruction based on retinotopic and functional properties of single neurons in monkeys (Galletti et al., 1996; Gamberini et al., 2011, 2018). **(B)** Medial (left) and dorsomedial (right) views of cortical surface reconstructions of a human left hemisphere (LH). In cyan the long pointing-selective strip of cortex from previous fMRI studies (e.g., Tosoni et al., 2015) superimposed over a posterior-medial view of the Conte69 atlas (Van Essen et al., 2011). This pointing-selective strip is rendered along with the borders of the average extent and location of areas V6, V6Av and V6Ad as defined by wide-field retinotopy and functional scans (Pitzalis et al., 2006, 2013d; Tosoni et al., 2015). Mean MNI coordinates of centers of mass and corresponding Brodmann area (BA) for the three regions are as follows: V6 (x y z; Brodmann area x), V6Av (x y z; Brodmann area x), V6Ad ($x = -9 \pm 4$, $y = -78 \pm 4$, $z = 43 \pm 6$; BA 7). The fundus of main sulci is indicated using dotted line and labelled as follow: Pos, parieto-occipital sulcus; SPs, sub-parietal sulcus; Cgs, cingulate sulcus; *a* anterior, *v* ventral, *p* posterior, *m* medial.

includes the human homologue of V6Av and V6Ad in its posterior part, likely includes the homologues of other macaque areas, such as area PEc, in its anterior part.

However, little attention has been given to the representation of lower limbs in the part of the SPL, that is posterior to the well-known somatotopic map in S-I, perhaps for the intrinsic difficulty in studying such a type of movement in the MR scanner. So far, only a few fMRI studies have compared hand and foot pointing movements in an attempt to find effector selectivity responses in the SPL (Heed et al., 2011, 2016; Leoné et al., 2014). They did not find clearly segregated effector-related responses, rather the revealed an activation in the anterior SPL associated with either hand and foot pointing movements. Only one study (Huang et al., 2012) using a *passive* stimulation, reported a somatotopic representation of the lower limb in the medial posterior parietal cortex (PPC) behind S-I. However, it is unknown whether this region corresponds to macaque area PE or PEc, or to neither of the two, because its functional profile with respect to active limb movements or other tasks that could specifically activate either area has never been tested.

Since here we did not perform a mapping of the entire body representation, we focused the present study on looking for the human homologue of macaque PEc, where upper and lower limbs and trunk are well represented, though not somatotopically organized (Gamberini et al., 2018). We use a combined approach of individual surface-based analysis of fMRI data, task-evoked activity (including somatomotor, visuomotor, and visual tasks) and resting-state functional connectivity. We aimed to identify a region with anatomical location, functional properties and cortical connections similar to those of macaque PEc. Since macaque PEc hosts a lower limb representation, we investigated lower limb movements using a novel set-up allowing subjects to perform controlled leg movements in the scanner.

These experiments uncovered the existence of a region (hPEc) responding to lower limb movements, located in between posterior (V6Ad) and anterior (PE and S-I) regions of the medial PPC. Despite their close vicinity, all these regions exhibited different functional profiles and cortico-cortical connections. The newly defined region encodes signals from different sensory modalities as well as motor signals. We propose that hPEc integrates visually derived self-motion signals with motor leg movement to guide locomotion and to intercept or avoid visual targets during locomotion.

2. Materials and methods

2.1. Subjects

Thirty-one right-handed healthy adults (17 females, mean age 27 years, s.d. 5.6) participated in this study. All subjects participated to both somatomotor and visual tasks while a sub-sample of 20 subjects (12 females, mean age 26 years, s.d. 5.9) also participated to the visuomotor task and underwent the resting-state scans. Two subjects were excluded from the visual task because of technical problems in data collection. All participants had normal or corrected-to-normal vision and no previous history of psychiatric or neurologic disease. Hand and foot right-dominance were tested by the Edinburgh handedness inventory (Oldfield, 1971). All subjects gave written informed consent. The project was approved by the Ethics Committee of Fondazione Santa Lucia, Rome, Italy.

2.2. Stimuli and experimental paradigm

Each participant completed in different days four fMRI sessions during: (a) a somatomotor task implying active movements of the inferior (leg) and superior (arm) limbs (Fig. 2A and B), designed to maximally activate leg and arm movement-related cells in the dorsomedial SPL; (b) a visuomotor task (delayed eye/hand/foot pointing; Fig. 2C) designed to reveal the responsiveness of the dorsal precuneus to spatially-directed pointing movements and to isolate effector-selective representations in the parietal cortex; (c) a visual task (Flow Fields; Fig. 2D), which we have previously proposed as a functional localizer for human V6, used here to reveal visual motion-related responses in the cortical PEc; (d) a series of resting-state scans while subjects were lying at rest with closed eyes and no experimenter-imposed task to explore the intrinsic whole-brain functional connectivity.

Somatomotor task (Active Leg/Arm movement scans; Fig. 2A and B). Each scan included seven leg and seven arm movement blocks lasting 20.5 s each, arranged in a pseudo-random sequence and interleaved with 14 fixation periods of variable duration (12, 14 or 16 s). Participants initially maintained central fixation on a white cross while keeping the right hand in the middle of the chest and both legs laid down on the scanner bed. Each block started with a written instruction ("Fix", "Leg" or

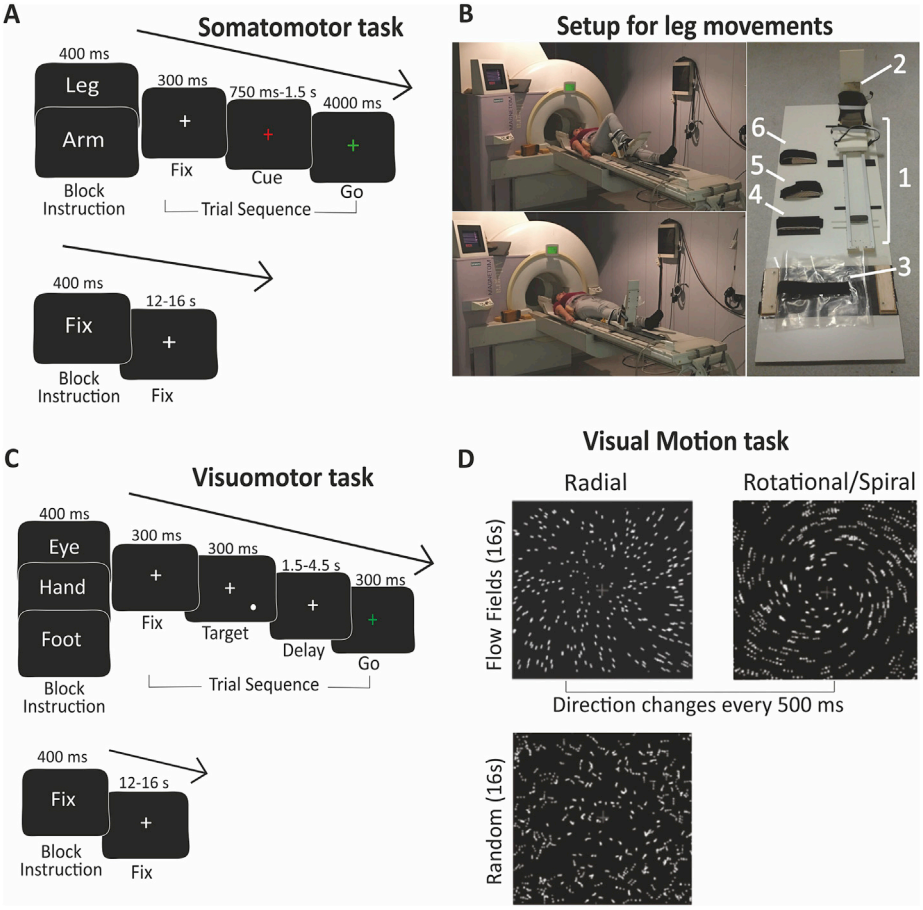

Fig. 2. Experimental task and set-up. (A) In the somatomotor task, subjects alternated block of leg or arm movements with passive fixation blocks. **(B)** A subject lying supine in the MRI scanner and performing a sequence of up *(left, upper panel)* and down *(left, lower panel)* leg movements using the in-house MRI-compatible set-up (*right panel*). Subject laid down on a wooden table, which perfectly fit the scanner bed, with his right leg extended along an aluminium-track (1) and with his foot comfortably fixed to the aluminium support (2) which sliding along the track allowed fluid and controlled leg movements. Velcro straps for immobilizing hip (3), tight (4), knee (5) ankle (6) of the left leg controlled for whole-body movements. **(C)** In the visuomotor task, subjects alternated blocks of memory delayed eye, hand or foot pointing movements to peripheral visual targets with passive fixation blocks. **(D)** In the visual motion task, blocks of coherently moving fields (Flow Fields) were interleaved with blocks of randomly moving fields.

"Arm") appearing for 400 ms at the center of the screen to inform on the task to be performed. During fixation blocks, the white central cross remained on the screen and subjects were asked only to maintain fixation throughout the block. In leg and arm blocks, each trial began with the white fixation cross turning red (cue signal for the movement preparation phase) for a variable delay (750, 1000, 1250, 1500 ms), and turning green (go signal) for 4 s. At the go signal, participants started a 4 s sequence of limb movements while keeping central fixation. Specifically, leg movements consisted in two phases: 1) a 2 s "forward phase" of rightward rotation of the right leg followed by leg flexion; and 2) a 2 s "backward phase" of leftward rotation of the right leg followed by leg extension to return at the initial resting position (see Fig. 2B; left panels). Arm movements consisted in a sequence of two phases: a 1) a 2 s "forward phase" of outward-rotation of the right hand/wrist followed by abduction of the right arm diagonally-directed to reach the opposite shoulder; and 2) a 2 s "backward phase" of inward-rotation of the right hand/wrist followed by arm adduction to return at the initial resting position at the centre of the chest. In both cases, the next trial started after an inter-trial interval of 1 s. Each block instruction was followed by four consecutive trials, and each trial consisted of a single 4 s sequence of leg or arm movements. The joint rotation of upper and lower limbs was introduced as an expedient to maximally activate the somatomotor cells of the dorsomedial parietal regions (where the leg is likely represented). Both limb movements in the somatomotor task were aimed towards a tactile target (this is why the task is called somatomotor): for the arm movement, the target was a foam rubber shaped as a ball positioned on the subject's left shoulder, at the most reachable position for him/her; for the leg movement, the foam rubber was positioned along the track at the point where the leg flexion reached its maximum, depending to the subjects' height (the foot moved along an average distance of 45 cm, range 35–55 cm). Before entering the scanner, participants were instructed on movement timing and sequence; then, in the scanner, they performed a short warm-up phase to familiarize with the tasks and the correct movement execution with the experimenter checking the performance. During the preliminary training session, the target positions were slightly adjusted for each individual subject until the movement was correctly performed without any discomfort. For leg movements, the training in the scanner consisted in learning to execute the movement as fluidly and naturally as possible without moving other body parts. For arm movements, the training consisted in learning to extend the arm enough to obtain the complete ipsilateral shoulder capsule rotation.

Visuomotor task (Eye/*Hand/Foot pointing scans;* Fig. 2C). Each scan included four eye, four hand and four foot-pointing blocks lasting 18 s each, arranged in a pseudo-random sequence and interleaved with 11 fixation periods of variable duration (12, 14 or 16 s). Initially, participants maintained central fixation while holding a button down with their right index and a foot pedal down with their right foot. Each block started with a written instruction ("Fix", "Eye", "Hand", and "Foot") appearing for 400 ms at the centre of a screen to inform about the task to be performed, followed by four trials. Each trial began with a peripheral target appearing for 300 ms, followed by a variable delay (1.5, 2.5, 3.5, or 4.5 s), after which the fixation point turned green (go signal) for 300 ms. Since visual stimuli were seen through a mirror (see below for more details), targets appeared as if they were positioned in front of the subjects, just above their heads. Note that in all cases, at the go signal participants performed the movement towards the *remembered* target position (since the target was not present anymore). In eye blocks, at the go signal participants performed a saccadic eye movement towards the remembered target position while continuing to hold both hand and foot-response buttons. In hand/foot blocks, at the go signal participants released the button/pedal and pointed the hand/foot to the remembered target location while keeping central fixation. In all cases participants

immediately returned to the starting position with the eyes/hand/foot, and the next trial started after 3.5 s. Instructions emphasized movement speed and spatial accuracy, and subjects were encouraged to prepare the movement as soon as the cue appeared. Targets were filled white circles of 0.9° diameter appearing in one of 8 radial locations at 4° of eccentricity. During fixation blocks, no target stimulus appeared, and subjects were asked to maintain central fixation throughout the block.

Given their critical role in this work, the required hand and foot movements are here described in detail. Hand pointing movements consisted in releasing the button, extending the right index and rotating the wrist to point to the remembered spatial location of the peripheral target shown on the screen, and then in rotating the wrist back downward, back to the starting position and holding down the button. Foot pointing movements consisted in releasing the foot pedal while rotating the ankle to point to the remembered spatial position of the target shown on the screen with the extended right big toe, then rotating the ankle downward back to the starting position and finally holding down the pedal. As in the somatomotor task (described above), during the execution of hand and foot pointing movements, subjects were explicitly requested to refrain from any other body movements (shoulder, arm, forearm and left leg) and to rotate only their wrist and ankle, respectively, as these are critical features for activating monkey PEc (Breveglieri et al., 2006, 2008; Gamberini et al., 2018; Fattori et al., 2009).

Visual motion task (*Flow Field scans;* Fig. 2D). Participants passively observed four 16-s blocks of coherently moving dot fields (Flow Fields), interleaved with four 16-s blocks of randomly moving dot fields, while maintaining central fixation. A new field of white dots was generated every 500 ms (dot size 0.4 × 0.4 deg^2). Dots immediately began to move along a trajectory so as to generate a coherent movement on a plane. The pattern motion was chosen randomly for that 500-ms period from a continuum ranging from dilation to outward spiral, to rotation, to inward spiral, to contraction. The center of the movement was jittered from flow to flow, and the speed varied within a small range. During the scrambled OFF period, dots and their movement vectors were generated as during the coherent ON periods except that each dot trajectory was rotated by a random angle around the pattern center before execution. This scrambled the coherency of movement (at a given point, dots moved in different directions) but preserved the speed gradient (central dots still moved slower than peripheral dots). The stimulus, which has been described also elsewhere (e.g., Pitzalis et al., 2010, 2012, 2013a; Serra et al., 2019), was presented in full view spanning at the most 66 by 47 degrees of visual angle.

2.3. Experimental set-up

To perform the somatomotor task (active leg/arm movements), we built an in-house MRI-compatible set-up allowing subjects to perform controlled leg movements (Fig. 2B, right panel) consisting in a removable aluminium track (Figs. 2B-1) fixed via Velcro straps on a wooden table perfectly fitting the scanner table. The movement guide ended with a foot aluminium support (Fig. 2B-) that comfortably enclosed the right foot and enabled fluid and controlled right leg movements sliding along the whole track. Whole-body movements were controlled and reduced as much as possible by immobilizing the hip (Figs. 2B-3), the thigh (Figs. 2B,3,5), the knee (Figs. 2B,3,5,6), and the ankle (Figs. 2B,3,5-7) of the left leg via Velcro straps. The above-described apparatus allowed participants to perform fully controlled real long-range active leg movements rather than simpler toe/ankle movements, as carried out in previous studies (e.g., Heed et al., 2011, 2016; Leoné et al., 2014).

The somatomotor set-up was also used to assist the hand/foot movement during the pointing task, in which participants were asked to press MR-compatible push buttons with their right hand and foot (see above). Just before starting the task, the foot aluminium support (Fig. 2B-) was moved away and the participant's foot was positioned on the response foot box (not shown) in a comfortable position. To attenuate possible fatigue in keeping the position throughout the entire experiment, the box was fixed on a foamed wedge tilted at 45° and the leg was supported by a circular cushion under the knee. The response box for hand-pointing task was placed at level of right hip and then fixed at the MRI table by tape. All those cautions avoided possible box displacements during the experiment.

In all tasks, we tried to prevent/control head movements in different ways. First, each subject performed a preliminary intensive training before the scanning session, lasting about 30 min. During the training subjects, lying on the scanner bed, had to familiarize with the set-up while performing the somatomotor and visuomotor tasks under visual control of an experimenter, which provided feedback about the possible occurrence of the head movements (especially those synchronized with the limb movements). After the training sessions, subjects learnt how to stay the most still as possible. Second, subjects' head was stabilized with foam padding and the head alignment was held constant by a chin-neck rest to minimize movement during the scans. The chin-neck rest was constituted by a soft cervical collar, made of soft foam, supporting the subject' neck and chin. The cervical collar rested on the subject' chest greatly reducing head movements along the pitch axis. In addition, we placed a circularly shaped foam cushion under the subject's inion and we positioned additional foams under the participant's back to reduce possible head movements due to discomfort.

Visual stimuli were generated by control computers equipped with a standard 3D graphic card located outside the MR room and running an in-house software (Galati et al., 2008) implemented in MATLAB (The MathWorks Inc., Natick, MA, USA). In the visual task, we used a wide field set-up similar to that originally described by our group (e.g., Pitzalis et al., 2006, 2018; Strappini et al., 2015, 2016). Shortly, an LCD video projector with a customized lens projected the visual stimuli onto a back-projection screen attached to the back of the head coil, at a distance of about 21 cm from the subjects' eyes and seen in binocular view via a large mirror enabling the vision of the whole screen. Nevertheless, subjects could comfortably fixate a central point on the screen without any visual discomforts (like blurring). Subjects' head was lowered of about 4 cm from iso-center so that even the bottom portion of the screen could be seen.

2.4. Behavioral measurements

During the somatomotor task, where no behavioural responses were recorded, an experimenter visually monitored the subjects' limb movements during the fMRI experiment to ensure that subjects correctly followed the instructions and performed arm or leg movements as indicated in the trial list.

During the visuomotor task, we recorded behavioral responses with respect to hand and foot pointing movements. Reaction times (RTs) were recorded as hand- and foot-related button releases connected to the control computer via optic fibers. Performance accuracy was assessed based on the proportion of correct trials, that is, trials in which movement was executed by the instructed effector. The RTs represent a measure of the performance accuracy only in terms of which *effector* was used by the subjects during each trial, but we do not have measures about the accuracy of the pointing *direction* during the fMRI experiment.

2.5. Eye tracking

An infrared ASL eye-tracking system operating at 60 Hz (Applied Science Laboratories, Bedford, MA; Model 504) was used to monitor gaze stability during fixation. Before the experiment, the eye position was calibrated through a nine-point calibration procedure and further controlled with a three-point calibration. We calculated the standard deviation of the right eye position averaged along both the horizontal and vertical dimensions (in degrees of visual angle) as a measure of fixation stability. The eye-tracker system was not compatible with the wide-field set-up, so we only monitored fixation during the somatomotor and the visuomotor scans. We obtained reliable data in a subset of subjects

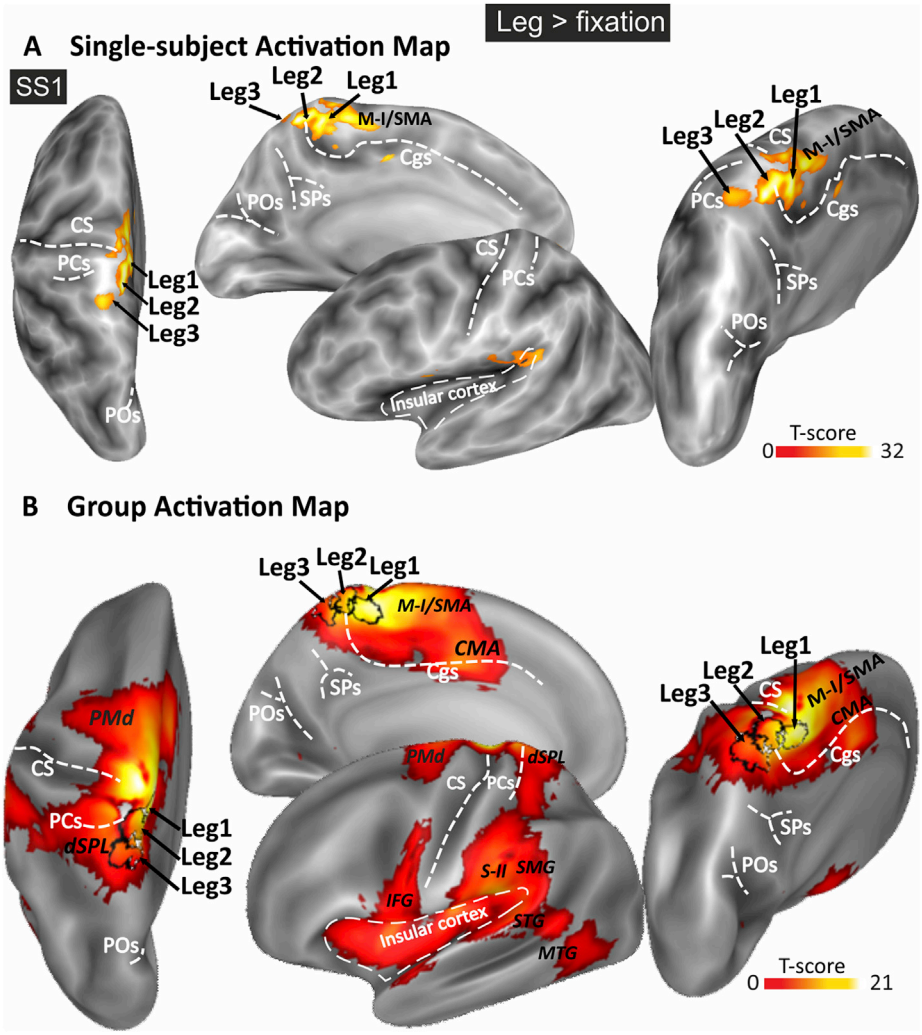

Fig. 3. Somatomotor task: three leg-related regions. Functional activation maps in the contrast "Leg > Fixation". **(A)** Single subject activation map displayed on the cortical surface reconstruction of the left hemisphere of a representative subject (SS1). **(B)** Group activation map displayed on the left hemisphere of the Conte69 atlas brain. In A and B, activation maps are rendered in superior, medial, lateral and dorsomedial views. Areas more active during leg movements are labelled: M-I, primary motor cortex; SMA, supplementary motor area; CMA, cingulate motor area; dSPL, dorsal superior parietal lobule; PMd, dorsal premotor area; SMG, supramarginal gyrus; S-II, secondary somatosensory cortex; STG, superior temporal gyrus; IFG, inferior frontal gyrus; MTG, middle temporal gyrus. Light and dark grey respectively represents gyri and sulci. The fundus of main sulci is indicated using dotted line and labelled as follow: POs, parieto-occipital sulcus; PCs, postcentral sulcus; CS, central Sulcus; SPs, subparietal sulcus; Cgs, cingulate sulcus. The color scale in A and B indicates the statistical significance of the activations using the FDR corrected p-values.

(N = 13, somatomotor task; N = 11, visuomotor task) for which statistics are reported in the results sections. Useable data was not obtained for every subject due to difficulties in maintaining pupil tracking across the experiment in light-eyed subjects and with an off-axis light path necessitated by larger visual field coverage. Gaze position was also visually inspected on-line to detect unwanted saccades during Hand/Foot pointing or fixation blocks and missed saccades during the Eye pointing blocks. This on-line control allowed us to give subjects feedbacks on excessive blinking or sign of lapses in attention at the end of the run acquisition.

2.6. Image acquisition and preprocessing

MR images were acquired at the Santa Lucia Foundation (Rome, Italy) on a 3T Siemens Allegra MR system in 20 of the 31 subjects that participated in the study, and on a Philips Achieva 3T scanner for the remaining 11 subjects. While data from the somatomotor and visual tasks were collected on both scanners, data from the visuomotor task and resting state scans were collected only from one scanner (Siemens Allegra). As a preliminary step we controlled for this factor by adding the scanner as between-subjects in the ANOVA analyses for only the two tasks where we combined data from two different scanners (i.e., somatomotor and visual task). In both these tasks, we found no significant main effect of scanner (all $F < 2$; $p > 0.05$), neither a significant scanner interaction (all $F < 2$; $p > 0.05$) with region (hPEc, PE, S-I) and condition (leg, arm) in the somatomotor task and with region in the visual task. Both scanners were equipped for echo-planar imaging and a standard head coil was used. In the 3T Siemens Allegra MR system we used a receiving/transmitting head coil, while in the 3T Philips Achieva system we used a 32-channel head coil. Functional T2*-weighted images were collected using a gradient echo EPI sequence using blood-oxygenation level-dependent imaging (Kwong et al., 1992). For scans collected on the Siemens Allegra 3T scanner, thirty contiguous 3.5 mm slices were acquired in the AC–PC plane with an in-plane resolution of 3 × 3 mm and an interleaved excitation order (0 mm gap), 64 × 64 image matrix, echo time (TE) = 30 ms, flip angle = 70°, repetition time (TR) = 2 s. From the superior convexity, sampling included all the cerebral cortex, excluding only the ventral portion of the cerebellum. For scans collected on the Philips Achieva 3T scanner, imaging parameters were as follows: TR: 2 s, TE: 30 ms, 38 slices acquired in the ascending order with 1 mm gap, voxel size 2.5 x 2.5 × 2.5 mm, flip angle = 77°.

Structural images were collected using T1-weighted sequence. For the Allegra scanner a sagittal magnetization-prepared rapid acquisition gradient echo (MPRAGE) sequence was used with following parameters: TR = 2 s, TE = 4.38 ms, flip angle = 8 deg, 512 × 512 image matrix, 0.5 × 0.5 mm in-plane resolution, 176 contiguous 1 mm thick sagittal slices. For the Achieva scanner a turbo field echo sequence (TFE) was used with following parameters: TR = 0.04 s, TE = 5.84 ms, flip angle = 8 deg, 512 × 512 image matrix, 0.5 × 0.5 mm in-plane resolution, 342 contiguous 1 mm thick sagittal slices).

In each scan, the first four volumes were discarded from data analysis to achieve a steady state, and the experimental tasks started at the

beginning of the fifth volume. Overall, each subject completed two 256-s long Flow Field scans, three 402-s long pointing scans, two or three 526-s long active movement scans and, two 256-s long resting-state scans.

Structural images were analyzed using FreeSurfer 5.1 (http://surfer.nmr.mgh.harvard.edu/) to obtain a surface representation of each individual cortical hemisphere in a standard space. We used the "recon-all" fully automated processing pipeline, which, among other steps, performs intensity correction, transformation to Talairach space, normalization, skull-stripping, subcortical and white-matter segmentation, surface tessellation, surface refinement, surface inflation, sulcus-based nonlinear morphing to a cross-subject spherical coordinate system, and cortical parcellation (Dale et al., 1999; Desikan et al., 2006). Each hemisphere was then completely flattened using five relaxation cuts: one cut along the calcarine fissure, three equally spaced radial cuts on the medial surface, and one sagittal cut around the temporal lobe. The resulting surface reconstructions were transformed to the symmetrical FS-LR space (Van Essen et al., 2012) using tools in the Connectome Workbench software (https://www.humanconnectome.org/software/get-connectome-workbench), resulting in surface meshes with approximately 74K nodes per hemisphere.

Functional images were realigned within and across scans to correct for head movement and coregistered with structural MPRAGE/TFE scans using SPM12 (Wellcome Department of Cognitive Neurology, London, UK). Functional data were then resampled to the individual cortical surface using ribbon-constrained resampling as implemented in Connectome Workbench (Glasser et al., 2013) and finally smoothed along the surface with an iterative procedure emulating a Gaussian kernel with a 6 mm full width at half-maximum (FWHM).

2.7. Head movements during fMRI acquisitions

Although we tried to reduce head movements in different ways (see above), it is impossible to completely prevent them, especially because participants were requested to perform long-range limb movements. Thus, we performed a thorough assessment of how much subject were moving during the acquisitions and adopted a number of strategies to minimize the impact of head movement on signal quality. The quantity of head movement at each time point was quantified through the framewise displacement index (FD, Power et al., 2012), an estimate in mm of the head movement relative to the previous time point, computed as the sum of the absolute values of the differentiated realignment estimates. Supplementary Fig. 1 shows the across-scans average and standard deviation of FD as a function of time for all types of functional scans. As expected, head movement was conspicuous during the somatomotor task, prominently during the active blocks, with no apparent difference between leg and arm movement tasks; less evident during the visuomotor task, but during foot pointing blocks; and negligible during the visual motion and the resting state scans.

To more formally analyze differences across tasks, we analyzed FD as a function of task using scan-specific general linear models similar to those used to analyze the BOLD data (see next paragraph), but without convolving task predictors with the hemodynamic response function. Parameter estimates from individual general linear models were then analyzed at the group level through a series of paired t-tests, controlled for multiple comparisons ($p < 0.05$). Supplementary Fig. 2 shows the across-scans average and standard deviation of FD estimates as a function of task. In the somatomotor task, arm and leg movement blocks induced more head movement than baseline blocks, but importantly, subjects moved equally during arm and leg blocks ($t(67) = 0.284$, $p = 0.78$ uncorrected). Thus, importantly for the interpretation of the BOLD results interpretation, head movement cannot explain the different activity profile between the arm and the leg conditions in the somatomotor task. In the visuomotor task, foot pointing induced more movements than the other conditions.

Based on the above quantification of head movements, we performed a quality control based on the "censoring" approach suggested by Siegel et al. (2014): time points associated with an instantaneous head movement above a standard threshold (FD > 0.9 mm, Siegel et al., 2014) were marked as suspect in terms of the potentiality to induce motion artifacts. In the visuomotor, visual motion, and resting state scans there were only 12 suspect time points across the whole dataset (corresponding to 0.05%). In the somatomotor task there was an average of 2.14% (s.d. 4.01%) suspect time points per scan, but most of them were concentrated in 7 scans (out of 74) each exceeding 10% of suspect time points. After excluding these scans, the average in the remaining dataset was only 1.03% (s.d. 1.95%) of suspect time points per run. On the basis of such controls, we censored the possibly contaminated scans, which resulted in completely excluding three subjects who had undergone both the somatomotor and the visual tasks (only one of them had also undergone the visuomotor task and resting-state session). We further reduced the potential effects of head motion by adding the six cumulative head movement parameters (three translations and three rotations) and the FD values as nuisance regressors in the BOLD analyses (see below).

2.8. Statistical analyses of the task-evoked activity

Functional images were analyzed for each participant separately on a vertex by vertex basis, according to the general linear model, by modelling each "active" blocks as box-car functions, convolved with a canonical hemodynamic response function as implemented in SPM 12. Blocks of fixation were not explicitly modelled as GLM regressors and were thus treated as part of the residual variance. To further reduce motion-induced noise, six head movement-related regressors parameters (translations and rotations) and one additional regressor for FD (framewise displacement) values (see above) were also included in the model as nuisance regressors. We analysed the visual, somatomotor and visuomotor scans on a vertex by vertex basis, applying the GLM both to the surface-transformed smoothed fMRI images and to regional time courses, obtained by averaging the unsmoothed BOLD time series across vertices in specific cortical regions, as detailed below. For vertex-wise analysis, a parameter estimate was obtained for each subject and in each cortical vertex that represented the estimated signal change during active blocks relative to the baseline. Group-level statistical parametric maps were formed through one-sample t tests, comparing signal in each condition to the baseline, and through paired t tests, comparing signal among pairs of conditions, respectively. Statistical maps were corrected for multiple comparisons at the cluster level ($p < 0.05$) through a topological false discovery rate procedure based on random field theory (Chumbley et al., 2010), after defining clusters of adjacent vertices surviving at least an uncorrected voxel-level threshold of $p < 0.001$.

For regional analyses, we focused on individual Leg > Fixation maps to reveal brain regions exhibiting a clear leg-related representation in the somatomotor task. We defined distinct leg-related regions by isolating single activation peaks and their neighborhood through a watershed segmentation algorithm as applied to surface meshes (Mangan and Whitaker, 1999). Applying this procedure, we isolated, for each individual, three activation peaks (not always three distinct cluster of activations), located in primary somatosensory (Leg1) and precuneate cortices (Leg2 and Leg3).

For each region, subject- and condition-specific parameter estimates, representing the estimated signal change, were analysed as a function of somatomotor, visuomotor and visual tasks thus entering different ANOVAs (see below) with experimental conditions as factor in which subject was treated as a random effect.

In the somatomotor task, regional hemodynamic responses of the three leg-related regions were analysed with respect to the arm condition through a series of one-tailed *t*-test against zero in order to find any significant response also for upper limbs movements. We also conducted a one-way ANOVA with region as factor to assess any difference among the three leg-related regions. In the visuomotor task, a series of one-sample t-tests were used to assess the presence of reliable activation within the three leg-related regions during eye/hand/foot pointing

movements. We then performed a region by experimental condition ANOVA to explore any effector-related difference among the three regions. The three leg-related regions were also analysed as a function of the visual task through a series of one-sample t-tests, with the aim to reveal any significant response to the optic flow. We also conducted a one-way ANOVA with region as factor to reveal any difference among the three regions with respect to the Flow Field stimulation. For all the above-mentioned analyses, we applied a Bonferroni correction for multiple comparisons ($p = 0.05/N$; $N = 3$ in the somatomotor task; $N = 9$ in the visuomotor task; $N = 3$ in the visual task). P-values are meant as significant and Bonferroni-corrected when surviving to the calculated threshold, otherwise we refer to significant but Bonferroni-uncorrected p-values. For comparison, probabilistic regions of the two leg-related areas located in the precuneate cortex (Leg2 and Leg3) were created by combining individual regions across subjects. To anticipate, this procedure allowed us to evaluate the anatomical location of Leg3, the leg-related region that we propose to correspond to the human PEc (hPEc) and its relationship with the anterior Leg2, which we propose to correspond to the human PE (Huang et al., 2012).

Additionally, since the caudalmost position of the dorsal precuneus hosts the human V6Ad, thus potentially indicating the posterior border of the hPEc, we also created a third probabilistic region by combining the individual V6Ad areas, which were identified here using the visuomotor task by selecting for each participant all vertices more active during eye/hand/foot pointing than fixation baseline within the anterior POs (see Tosoni et al., 2015, for a similar procedure).

2.9. Statistical analysis of resting-state functional connectivity (fcMRI)

We examined the pattern of cortical connections associated with the two leg-related regions of the dorsomedial SPL (Leg3 and Leg2). The rationale behind this approach was to confirm that the most posterior leg-related region (Leg3) corresponds to the human homologue of macaque PEc, by demonstrating that this regions shows a pattern of cortical connections similar to those observed in the corresponding macaque area and belongs to a partially segregated network with respect to the surrounding regions, i.e., the anterior leg-related region (Leg2 or PE; Huang et al., 2012) and the posterior V6Ad (Tosoni et al., 2015).

To this aim, a connectivity analysis of the fMRI data recorded at rest was implemented using a seed-to-voxel approach in which a map of covariance was estimated from the BOLD signal time course extracted from each of the above-mentioned seed regions. fcMRI maps were obtained using voxel-wise multiple regression analysis (see Margulies et al., 2009; Uddin et al., 2010; Tosoni et al., 2015 for similar data analysis methods). The time course of each seed was used as a covariate of interest in a GLM applied at each hemispheric vertex. Sources of spurious variance were removed by including extra regressors as nuisance covariates: the global signal time course, estimated as the average BOLD signal within the default SPM within-brain mask, plus several other regressors summarizing vertex time courses in regions where the time series data are unlikely to be modulated by neural activity, to reduce noise due to physiological fluctuations and other sources, such as subject motion (Behzadi et al., 2007). In particular, we included four white matter and four cerebrospinal fluid (CSF) regressors, computed as the first four eigenvariates of a singular value decomposition of the resting state time courses of all voxels within the white matter and CSF, respectively. We also included six head movement regressors to further reduce motion-induced noise. Individual seed time courses were orthogonalized with respect to nuisance regressors. The GLM also included constant terms to model overall differences across scans. Images were temporally filtered using a band-pass filter with cut-off frequencies of 0.1 and 0.01 Hz before entering the GLM. The low-pass filtering was motivated by the fact that the majority of the previous fcMRI studies focused on slow (<0.1 Hz) BOLD fluctuations (see Fox and Raichle, 2007 for a review). For each model, first level, subject-specific GLMs were used to compute whole-brain regression parameter estimates reflecting the effect of each seed region regressor on each cortical surface vertex. At the second level, group fcMRI statistical maps were generated for hPEc and close regions (V6Ad and hPE) using one-tailed one-sample t tests in which subjects were treated as a random effect. The rationale behind this approach was twofold: (1) we wanted to further confirm the homology between the human and the monkey PEc region, identifying brain regions significantly connected with this region (Fig. 9); (2) we wanted to show that, even if close, regions were differentially connected with the cortical surface. For the second aim, we additionally performed formal comparisons between fcMRI maps through a series of two-tailed paired t tests comparing parameter estimates which reflected the cortical connections of the three neighbouring regions (V6Ad vs. hPEc, hPEc vs. hPE, V6Ad vs. hPE). These maps in Fig. 10 identify brain regions exhibiting different functional connectivity with the three seed regions. Group-level connectivity maps were corrected for multiple correction at cluster level ($p < 0.05$), after defining clusters of adjacent vertices surviving at least an uncorrected voxel-level threshold of $p < 0.005$.

To illustrate the relationship between our findings and the location of specific visual and motor areas, we overlaid the resulting connectivity maps onto the composite human cortical parcellation of the Conte69 brain atlas (Van Essen et al., 2011) including motor and somatosensory areas included in the Brodmann parcellation of the atlas. We are aware that these parcellations are typically based on retinotopic or functional data from single subjects or small groups of subjects, therefore the comparison between our group functional connectivity maps and areal borders from these parcellations are merely illustrative. We also overlaid the resulting connectivity maps onto the multi-modal parcellation of the human cingulate cortex from the Human Connectome Project (HCP) (Glasser et al., 2016). We also compared our results with the probabilistic scene-responsive region PPA (parahippocampal place area, Epstein and Kanwisher, 1998), by averaging individual functional ROIs from a separate set of 44 participants from our database who underwent a "localizer" fMRI experiment consisting in passive viewing of blocks of scenes vs. faces (see Sulpizio et al., 2013, 2014, 2018 for a similar procedure). Present data will be made available on request in compliance with the requirements of the funding institutes, and with the institutional ethics approval.

3. Results

3.1. Behavioural measures

In the active movement task, participants correctly moved always the effector as indicated by the instruction. In the pointing task, behavioural responses were recorded during hand and foot pointing in 16/20 subjects. Participants followed the instructions correctly in all pointing trials (see below for saccadic error rates). Mean RTs were 563 ms (SE ± 54 ms) for hand pointing and 628 ms (SE ± 30 ms) for foot pointing, values comparable to those obtained in previous studies (Beurze et al., 2007, 2009; Heed et al., 2011, 2016). The active movement task was simple to execute, not requiring a great attentional demand nor memory load. Indeed, all subjects performed active limb movement when expected with no exception, and never performed extra limb movements.

The eye movement data collected during the fMRI scanning in a subset of subjects (see Material and Methods) indicate that subjects accurately maintained fixation while performing the visuomotor and somatomotor tasks. The fixation stability was excellent (SD = 1.1° for the somatomotor task and 1.0° for the visuomotor task), well in line with standard parameters (e.g., Crossland et al., 2008; Di Russo et al., 2003; Fischer et al., 2012; Pitzalis et al., 2013d). Subjects were on average also quite accurate with respect to the saccadic performance. The percentage of unwanted saccades was low (3% in the somatomotor task and 1% in the visuomotor task). The percentage of missed saccades in the visuomotor task was low (4%). Since such saccades were rare and equally distributed across block types, we did not exclude the contaminated trials from the analysis. The observed extra saccades are not expected to result

in any systematic bias, but eventually in a decreased sensitivity in detecting differences between conditions.

3.2. Imaging results

3.2.1. Somatomotor task: three distinct leg representations in the human dorsomedial parietal cortex

We used the somatomotor task to explore the dorsomedial cortex of each subject looking for multiple cortical leg representations. Based on human data present in literature, we expected to find two regions representing the lower limbs in the dorsomedial cortex, one corresponding to the medialmost part of S-I and the other, posterior to S-I, to the medialmost part of the parietal homunculus described by Huang et al. (2012). As stated in introduction, it is unknown whether the parietal homunculus corresponds to macaque area PE or PEc, but in any case, only one representation of the lower limb was described so far in humans posterior to S-I. Here, instead, we found two leg representations in the cortical territory of the medial precuneus, posterior to S-I, similarly to what previously observed in the macaque brain (Gamberini et al., 2018; Seelke et al., 2012).

Surface-based regions reflecting leg representation in single-subject maps were identified by looking at all the activation peaks in the dorsomedial somatosensory/parietal cortex as resulting from the Leg > Fixation contrast map. Based on this procedure we identified in most of the subjects three leg-related activation peaks as illustrated in Fig. 3A on a representative subject (SS1) and in Fig. 4 on other nine subjects (SS2-10).

The most anterior peak (Leg1) was found in all subjects (28/28 hemispheres) on the medial portion of the brain surface, anterior to the dorsal tip of the cingulate sulcus and posterior to the dorsal tip of the central sulcus, the latter being the anatomical landmark of the primary motor region (M-I, indicated by label in Fig. 3A). The position of Leg1 described here fits with the location of leg and foot somatotopic representations in the primary somatosensory region found in previous fMRI reports (Di Russo et al., 2006; Golaszewski et al., 2006; Huang et al., 2012; Akselrod et al., 2017). Note in this respect that, while the somatotopic representations of other body parts (as face, hand, fingers etc.) are more commonly studied (e.g. Besle et al., 2013; Sanchez-Panchuelo et al., 2012, 2014; Martuzzi et al., 2014; Nelson and Chen, 2008), fMRI reports on the somatotopic representation of the lower limb in S-I is scarce, and the medial end of the human S-I (where the foot is represented) is rarely reported (but see Di Russo et al., 2006; Akselrod et al., 2017; Tal et al., 2017).

Posterior to the first peak, a second peak (Leg2) was found in 28/28 hemispheres on the exposed dorsomedial surface of the anterior SPL, right over the dorsal tip of the cingulate sulcus. Relative to the postcentral sulcus (PCs), Leg2 was typically positioned either medial to the medial end of it (or it was anterior to it) in 26/28 (see SS1 in Fig. 3A); only in 2/28 hemispheres Leg2 was found posterior to the postcentral sulcus (see SS5 in Fig. 4). Relative to Leg1, Leg2 was typically positioned along a similar z axis (see SS1 in Fig. 3A and SS2-3-4-6-7-8-10 in Fig. 4). The location of this region falls within the parietal homunculus found by Huang et al. (2012), in correspondence of its lower limb representation (leg and foot).

Posterior to the second peak, a third peak (Leg3) was found in 26/28 hemispheres in the anterior part of the dorsal precuneus. In all subjects, Leg3 was located anterior to the subparietal sulcus (SPs) and posterior to the ascending ramus of the cingulate sulcus. Relative to the postcentral sulcus, Leg3 was located posterior to it in almost all subjects (24/26) and rarely medial to the medial end of it (2/26). As the Leg3/Leg2 relationship, Leg3 was typically positioned either dorsal to Leg2 (see SS1 in Fig. 3A and SS2-3-4-5-7-8-9-10 in Fig. 4) or along a similar z axis (see SS6 in Fig. 4). Notably, we never observed leg-related functional activation behind Leg3, which constitutes the very most posterior functional peak we could observe during the somatomotor task. The size (number of nodes) and the anatomical location (MNI coordinates and corresponding Broadman Areas, BA) of each region are listed in Table 1.

Fig. 3B shows group contralateral activation map for the Leg > Fixation contrast overlaid onto atlas Conte69 (see also Supplementary Table 1 for details and Supplementary Fig. 3 for the ipsilateral activation map). Regions exhibiting significant responses to long-range leg movements compared to the baseline fixation are part of a wide network of parietal, frontal and temporo-insular regions involved in active lower limb movements. Activation encompassed the primary motor and somotosensory cortices (M-I and S-I), the dorsal premotor cortex (PMd) and extended laterally into the inferior frontal gyrus (IFG) and medially into the supplementary motor area (SMA) and the adjoining middle cingulum including the cingulate motor area (CMA). The cortical activation extended posteriorly from the cingulate sulcus into the anterior part of the precuneus and laterally around the postcentral sulcus in the dorsal part of the superior parietal lobule (dSPL). Strong activations were also observed at the intersection of parietal, temporal and insular cortices, so that to include the supramarginal gyrus (SMG), the secondary somatosensory cortices (S-II), the middle and superior temporal gyrus (MTG/STG), and the insula, in both its anterior and posterior division. The activation in the posterior insula probably corresponds to the parietal insular or PIC area and to the parietal insular/vestibular or PIVC area (Frank et al., 2016).

To strengthen subject-based results, the average anatomical position of the three leg-related regions (indicated by a black outline) were overlaid onto the leg activation group map (Fig. 3B). Notably, both subject-based (Fig. 3A) and group-based activation maps (Fig. 3B) showed that the cortical territory behind Leg3, including the posterior precuneus dorsally, the POs medially and the intraparetal sulcus laterally, is totally unresponsive to active leg movements. This connotes Leg3 as the first station for leg representation in the dorsal precuneate cortex. Notable, the third peak (Leg3) was less recognizable as a separate area in the group-based activation maps (Fig. 3B), reinforcing the importance of individual surface-based analysis of fMRI data to isolate different leg-related regions in the dorsal SPL.

3.2.2. Somatomotor task: arm-related responses within the three leg-related regions

While the most anterior leg representation (Leg1) corresponds to the cortical territory representing lower limbs in S-I, it is an open question to which regions correspond the intermediate Leg2 and the posterior Leg3.

Thus, to better characterize the somatomotor properties of these leg-related regions, we further explored their response to long-range active arm movements. The rationale of this approach was to look for a region responding to both upper and lower limb movements, as it is the case for the monkey PEc area. The mean percent signal changes observed in each of these regions during the somatomotor task are plotted as a function of leg and arm movements in the column histograms of Fig. 5A. First, we performed a series of one-tailed *t*-test against zero to assess any different activation in the arm condition with respect to the baseline (fixation). We found a significant arm-related positive activation only in Leg3 ($t_{25} = 4.01$, $p = 0.005$), while Leg2 did not show any significant response to arm movements ($t_{27} = 0.74$, $p = 0.46$), and Leg1 (S-I) showed a significant arm-related deactivation ($t_{27} = -4.40$, $p = 0.0002$). A repeated measures ANOVA with region (Leg1, Leg2, Leg3) and condition (Leg, Arm) as factors confirmed functional differences between areas, revealing a significant region by condition interaction ($F_{2,48} = 28.26$, $p < 0.0001$; $\eta_p^2 = 0.54$) indicating that Leg3 responded stronger to active arm movements as compared to both Leg2 ($p = 0.01$) and Leg1 ($p = 0.0001$). More generally, in the arm condition we observed an increase of activity along the anterior-to-posterior axis (Leg3 > Leg2 > Leg1; $p < 0.05$).

Based on their anatomical position and their response to arm movements, Leg2 and Leg3 might correspond to the human homologue of macaque PE and PEc, respectively. Their response profile mirrored that observed in the corresponding macaque areas: while Leg2 did not show any arm-related response, thus probably corresponding to the leg

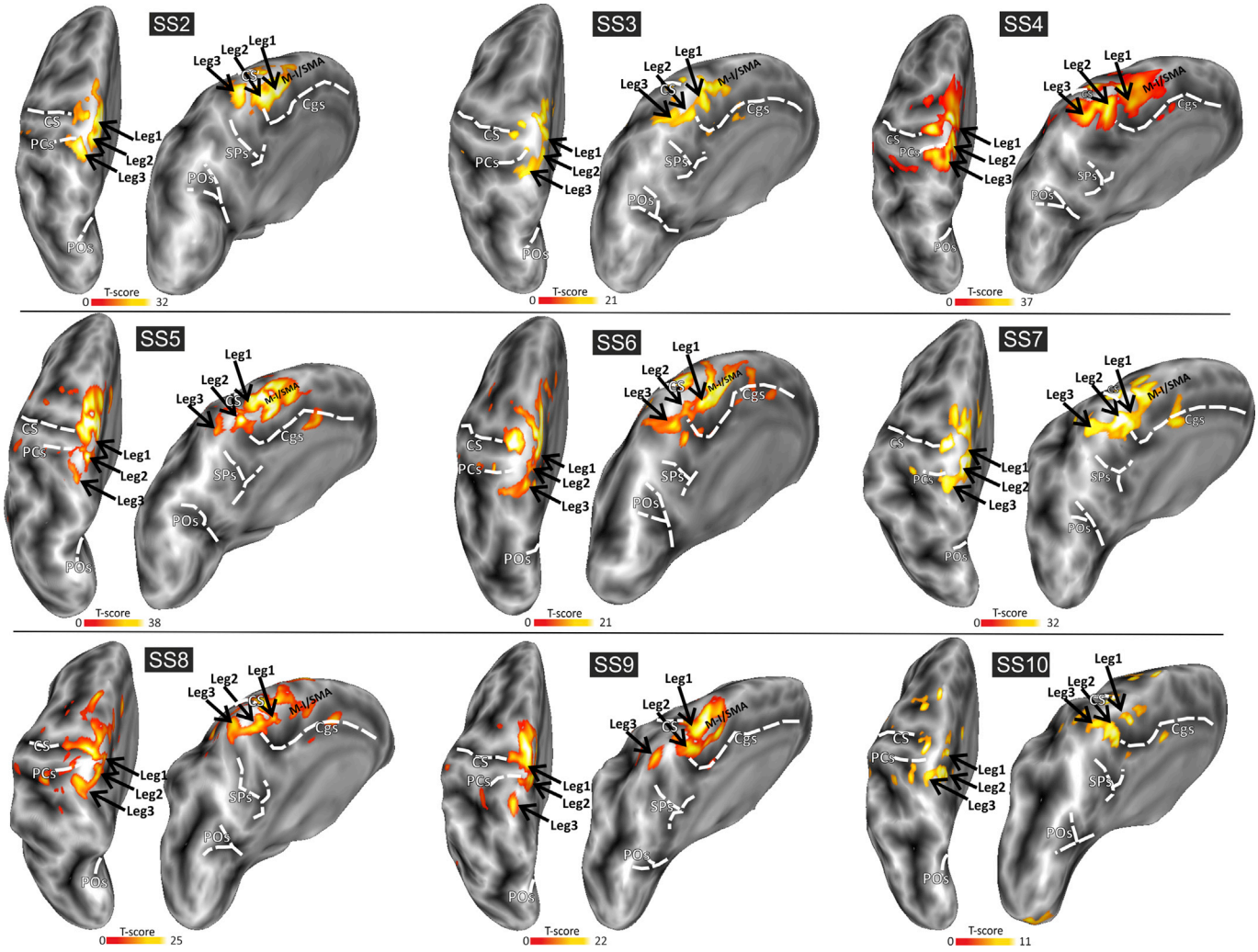

Fig. 4. Somatomotor task: three leg-related regions. Functional activation maps in the contrast "Leg>Fixation". Single subject activation map displayed on the cortical surface reconstruction of the left hemisphere of nine representative subject (SS2-10). Areas more active during leg movements are labelled: M-I, primary motor cortex; SMA, supplementary motor area. Light and dark grey respectively represents gyri and sulci. The fundus of main sulci is indicated using dotted line and labelled as follow: POs, parieto-occipital sulcus; PCs, Postcentral sulcus; CS, central Sulcus; SPs, sub-parietal sulcus; Cgs, cingulate sulcus. The color scale indicates the statistical significance of the activations using the FDR corrected p-values.

Table 1
Position: MNI coordinates (mm) of ROIs. Centers of mass of individually defined regions are reported, as values mediated across subjects. BA, Brodmann areas that each ROI falls on. Size: mean number of nodes (± standard deviation). Statistical significance: mean peak t-value (± standard deviation).

Region	MNI coordinates					
	x	*y*	*z*	*BA*	Number of nodes	Peak T-value
Leg1 (S-I)	−6±3	−36±8	58±3	BA 5	223±79	19.21
Leg2 (hPE)	−12±3	−50±5	66±5	BA 5	233±99	12.08
Leg3 (hPEc)	−13±5	−61±3	62±5	BA 7	183±107	8.55

territory of the somatotopic macaque PE (Seelke et al., 2012), Leg3 was a leg-related region responding also to arm movements, and thus not showing a clear somatotopy, as it is the case for macaque PEc (Breveglieri et al., 2006; Gamberini et al., 2018). Thus, although further evidence will be provided through the paper to corroborate this speculative hypothesis, for sake of clarity, hereafter we will call Leg2 and Leg3 as the leg territory of the putative human PE (hPE) and human PEc (hPEc), respectively.

Fig. 5 shows the Arm > Fixation contrast map at single subject (Fig. 5B) and at the group level (Fig. 5C; see also Supplementary Table 1 for details). Both single- and group-based activation maps revealed the involvement of a lateral portion of M-I and S-I, corresponding to the cortical territory where upper limbs are represented, and the adjoining PMd. This activation encompassed the postcentral sulcus and extended posteriorly into the dSPL and ventrally into the SMG, the somatosensory cortex S-II, the temporal gyrus or STG and partially the posterior insula. In the medial surface, we also found activation in the anterior CMA. Notably, as expected from the regional analyses (Fig. 5A), both subject-based (Fig. 5B) and group-based (Fig. 5C) revealed that the arm-related activation map did not include the two anteriormost leg-related regions (hPE and S-I) but only (partially) the most posterior leg-related region (hPEc).

In summary, among the three "leg" regions, hPEc is the only one responding to both arm and leg movements, as expected from single-cell recordings on monkey PEc (e.g., Breveglieri et al., 2006, 2008). The hPE and S-I respond only to leg movements (Figs. 3 and 4), but not to arm movement (Fig. 5), again as expected according to their somatotopic organization. Thus, the hPEc response profile observed during the somatomotor task suggests a homology with the monkey area PEc.

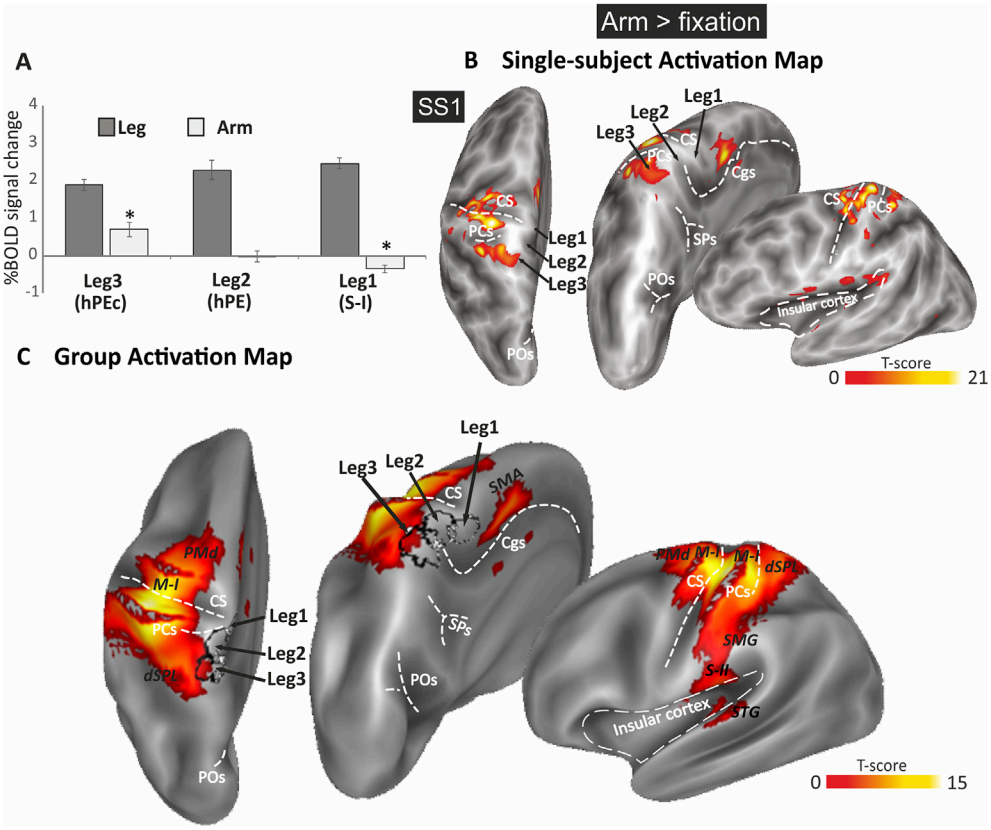

Fig. 5. Somatomotor task: arm-related responses within the three leg-related regions. Functional activation maps in the contras t "Arm > Fixation". **(A)** Plots show parameter estimates in each leg-related region for the leg (dark grey) and arm (light grey) conditions. Note that in SPM images these parameters represent % BOLD signal changes relative to an intra-cerebral mean. Asterisks refer to T-test versus zero. *p < 0.001. **(B)** Single subject activation map displayed on the cortical surface reconstruction of the left hemisphere of a representative subject (SS1). **(C)** Group activation map displayed on the left hemisphere of the Conte69 atlas brain. In B and C, activation maps are rendered in superior, dorsomedial and lateral views. Areas more active during arm movements are labelled as in Fig. 3. Other labels and logos are as in Fig. 3.

3.2.3. Visuomotor task: only hPEc responds to both hand and foot pointing

Macaque monkey area PEc is not only defined by its anatomical location and somatomotor properties (i.e. a region in the caudal aspect of SPL located in between V6Ad and PE, that responds to somatosensory stimulation of the upper and lower limbs; Breveglieri et al., 2006, 2008; Gamberini et al., 2018), but also by its responsiveness to spatially-directed eye and reaching movements (Hadjidimitrakis et al., 2015; Piserchia et al., 2017). Therefore, to bolster the notion of a homology between the monkey area PEc and the human PEc described here, we examined the magnitude of the evoked responses in hPEc, hPE and S-I to the visuomotor task. This analysis enabled us to evaluate whether hPEc exhibited 1) the same functional profile of the corresponding monkey area and 2) a distinct pattern of activity with respect to the other two leg-related regions.

The BOLD percent signal change for eye/hand/foot pointing blocks in the three leg-related regions (hPEc, hPE, S-I) are plotted in the column histograms of Fig. 6A. To test the hypothesis about the presence of hand- and foot-related positive responses, the percent signal change of the three leg-related regions was compared to zero using one-tailed *t*-tests. For the eye condition, only negative responses were observed (hPEc: $t_{15} = -2.77$; $p = 0.01$ Bonferroni-uncorrected; hPE: $t_{17} = -6.09$; $p = 0.0001$; S-I: $t_{17} = -6.56$; $p = 10^{-5}$). In the hand condition, the PEc was the only area showing a significant positive response ($t_{15} = 3.66$; $p = 0.002$) while hPE and S-I showed no significant ($t_{17} = -2.63$; $p = 0.02$ Bonferroni-uncorrected) or negative responses ($t_{17} = -5.58$; $p = 0.0001$), respectively. In the foot condition, all the above-mentioned regions exhibited very strong positive responses (hPEc: $t_{15} = 9.19$; $p = 10^{-6}$; hPE: $t_{17} = 7.69$; $p = 10^{-6}$; S-I: $t_{17} = 10.60$; $p = 10^{-7}$). Any difference in the effector-preference among these regions was further explored through a region (hPEc, hPE, S-I) by effector (eye, hand, foot) repeated-measure ANOVA. We found a significant interaction ($F_{4, 60} = 11.07$; $p < 0.0001$; $\eta_p^2 = 0.42$) indicating that the three leg-related regions differed only during hand pointing movements: hPEc responded stronger to both hPE ($p = 0.001$) and S-I ($p = 0.0001$).

Beyond the regional approach, a whole-brain analysis was conducted to have a general picture of brain regions involved in hand, foot and eye pointing movements (Fig. 6B and C; see also Supplementary Table 2 for details).

Fig. 6B shows Hand-pointing > Fixation (green) and Foot-pointing > Fixation (red) activation maps together with the centers of mass of hPEc, hPE and S-I marked by a black spot. In addition to areas responding to hand or foot-pointing stimulation, we also observed a wide network of cortical areas commonly activated by hand and foot pointing movements (yellow patches). In agreement with the regional analysis, this whole-brain analysis shows that while hPEc responds to both hand- and foot-pointing (the center of hPEc overlaps a yellow patch), hPE and S-I respond only to foot-pointing (the centers of hPE and S-I overlap the red patch). Beyond common activations, we also observed a functional segregation between hand and foot pointing. The cortical network for hand and foot pointing reflected the well-known lateral-to-medial hand-foot organization (Huang et al., 2012; Heed et al., 2011; Leoné et al., 2014). Hand pointing movements (Fig. 6B, green patches) primarily involved the lateral portion of M-I and S-I with the activation extending ventrally along the central sulcus. Hand-related activation was also found in the middle temporal cortex and probably included the visual motion areas MT and MST (Tootell et al., 1995). Foot pointing movements (Fig. 6B, red patches) mainly involved the medial portion of M-I and S-I and extended posteriorly up to the cingulate sulcus. Foot-related activation was also found in the posterior portion of the insular cortex.

Fig. 6C shows Hand-pointing > Foot-pointing (green) and Foot-pointing > Hand-pointing (red) contrasts. This contrast shows the presence of any cortical regions with a specific effector-preference. These more selective contrasts between effectors confirm the medio-lateral somatotopic trend already observed in Fig. 6B and, in addition, show that only a minority of regions survives in the map. Fig. 6C reveals that while hPEc, hPE and S-I respond more to foot-pointing than hand-pointing, no parietal regions posterior to hPEc exhibit an effector-preference either for foot or for hand. In agreement with previous

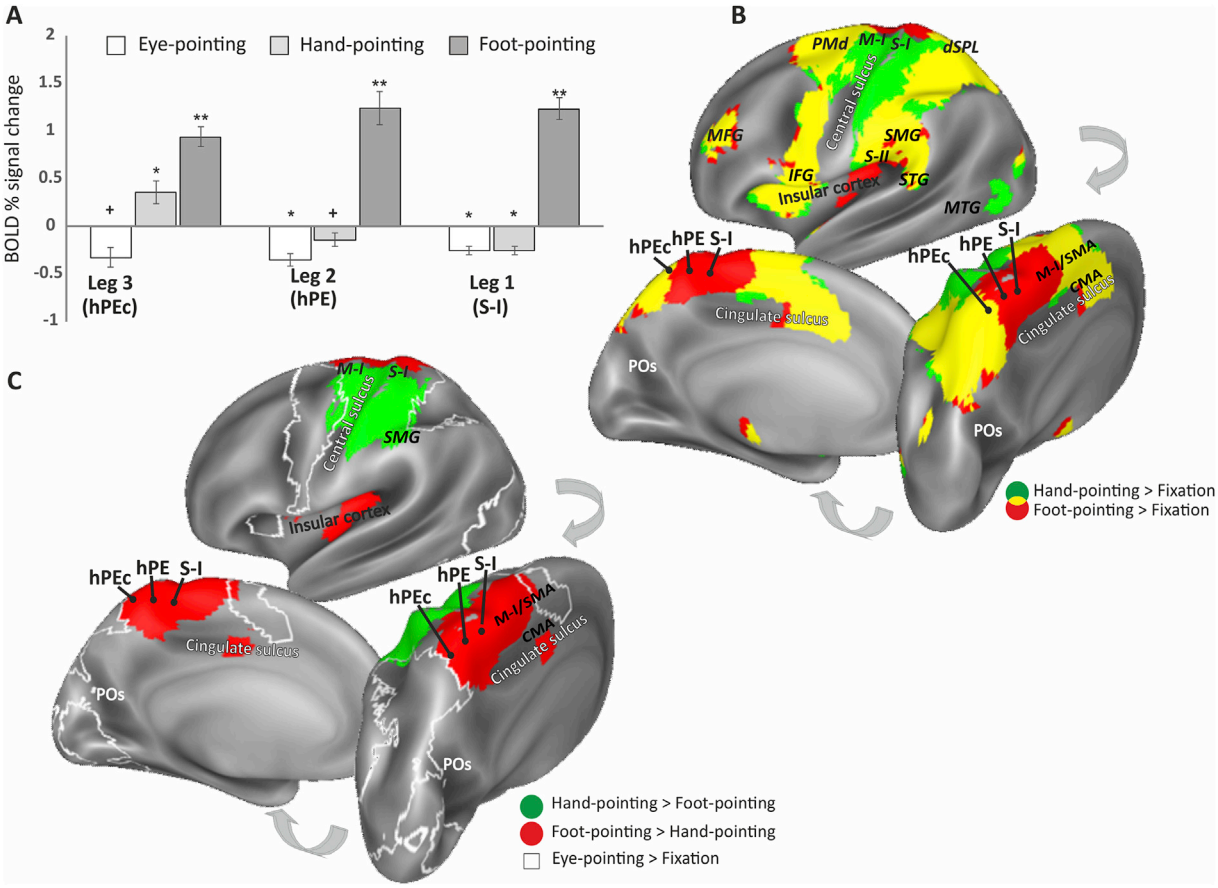

Fig. 6. Visuomotor task: hand and foot pointing related responses within the three leg-related regions. (A) Plots for each region indicates the averaged BOLD percent signal change ± standard error of the mean across subjects for each experimental condition: Eye-pointing (white), hand-pointing (light grey), foot-pointing (dark grey). Asterisks refer to T-test versus zero. **$p < 10^{-6}$; *$p < 0.001$; +$p < 0.05$, Bonferroni-uncorrected. **(B)** Group activation maps as resulting from hand-pointing > fixation (green) and foot-pointing > fixation (red) contrasts. **(C)** Group activation maps as resulting from hand-pointing > foot-pointing (green) and foot-pointing > hand-pointing (red) contrasts. The white outline indicates the cortical network activated by the saccade > fixation contrast. In B and C, activation maps are overlaid onto atlas Conte69 and rendered in three different inflated views (medial, lateral and dorsomedial). The centers of mass of hPEc, hPE and S-I are marked by a black spot. Other labels and logos are as in Figs. 3 and 5.

studies (Heed et al., 2011; Leoné et al., 2014), Fig. 6C clearly shows that a true effector preference is not widely distributed throughout all the brain and it does not involve posterior medial and lateral parietal regions.

As expected from the regional analyses, none of the three leg-related regions was part of the network of areas involved in saccade control. Notably, the cortical network for eye movements (Fig. 6C, white outline) did not include any of the three leg-related regions, nor the arm-related regions, but a wide distributed network of areas encompassing the striate and extrastriate visual cortex, the intraparietal sulcus (IPS) and the adjacent saccade-responsive areas (Sereno et al., 2001; Levy et al., 2007; Heed et al., 2011; Leoné et al., 2014) and the junction between the precentral and the superior frontal sulci, where the human Frontal Eye Field is probably located (Amiez et al., 2006). In this respect, the saccadic profile of the hPEc reported here is an original finding also with respect to single unit studies in the macaque.

In summary, we found that area hPEc has a unique functional profile, different from that observed in the neighboring regions hPE and S-I. While all three regions respond to foot pointing movements, only hPEc responds positively also to hand pointing. Moreover, since the cortical territory posterior to hPEc was silent in the contrast maps (Fig. 6C), area hPEc has a unique functional profile also with respect to posterior neighboring parietal regions.

3.2.4. *Visual task: only hPEc responds to optic flow*

To further support the homology between the monkey area PEc and the leg-related region described here, we examined whether the hPEc, similarly to the monkey counterpart, is involved in visual motion and optic flow processing (Squatrito et al., 2001; Raffi et al., 2002, 2010; 2011, 2014).

The BOLD percent signal change for flow field blocks (relative to random motion) in the three leg-related regions (hPEc, hPE, S-I) are plotted in the column histograms of Fig. 7A. The one-tailed t-tests against zero demonstrated that only the hPEc exhibited a significant response to optic flow ($t_{22} = 2.59$; $p = 0.02$). While hPE exhibited a marginal significant positive response ($t_{24} = 1.81$; $p = 0.08$), S-I did not show any significant response to flow fields ($t_{24} = 0.90$; $p = 0.38$). The one-way ANOVA confirmed a main effect of region ($F_{2,42} = 4.62$; $p < 0.05$; $\eta_p^2 = 0.18$), indicating that hPEc showed a stronger (but Bonferroni-uncorrected) response to flow fields as compared to both S-I ($p = 0.03$) and hPE ($p = 0.04$).

Fig. 7B shows the whole brain activation map for flow fields (relative to random motion) superimposed on the atlas brain (see also Supplementary Table 3 for details). This map included a wide network of activation in occipital, parietal, temporal and insular regions, where there are many well-known high-level egomotion regions (as V3A, V6+, IPSmot/VIP, CSv, pCi; e.g., Cardin and Smith, 2010, Pitzalis et al., 2010, 2013b,c; Serra et al., 2019). Most importantly for the present work, the flow field-related activation map includes the dorsalmost portion of the precuneate cortex, as expected from the regional analyses (Fig. 7A), which we hypothesized to host the human PEc, but not areas hPE and S-I.

This map includes also a large strip of cortex in the mesial, anterior part of the occipital lobe, that represents the far periphery of the visual field and that likely involves regions, such as the parahippocampal place area (PPA) at the boundary between posterior parahippocampal cortex and the anterior lingual gyrus, the retrosplenial complex (RSC) at the conjunction between the calcarine sulcus and the parietal-occipital sulcus (Epstein, 2008).

Notably, the wide visual motion stimulus we used was able to activate three multisensory regions primarily regarded as vestibular, 1) at the junction of parietal regions and insular cortex (probably including the posterior insular cortex or PIC; Frank et al., 2014), 2) in the postcentral sulcus (putative area 2v, p2v; Cardin and Smith, 2010) and 3) in frontal regions extending into the primary motor cortex and anterior to it (likely the human equivalent of the vestibular frontal area 3aNv, where the neck is represented; Guldin and Grüsser, 1998, for review; Smith et al., 2012).

3.2.5. *Anatomical location of hPEc and its relationship with the neighboring areas V6Ad and hPE*

To appreciate the human PEc anatomical location and its relationship with the neighboring areas, individual hPEc and hPE were combined across subjects to create probabilistic maps of location of the two leg-related regions and were projected onto the inflated Conte69 atlas surface (Van Essen et al., 2011). Since it has been recently shown that the caudalmost part of the dorsal precuneus hosts the human V6Ad (Tosoni et al., 2015, see Fig. 1B), which in macaque borders posteriorly the PEc (see Fig. 1A), we also created a probabilistic map of location of individual V6Ad (see methods for more information on V6Ad mapping) and projected it onto the atlas surface for a comparison (Fig. 8).

Fig. 8 shows the average location of three group-probabilistic regions. V6Ad (blue) is located in the posterior portion of the superior parietal lobule, in a cortical territory including the anterior bank of the dorsalmost POs and the caudalmost portion of the precuneate cortex (behind the subparietal sulcus). hPEc (green) occupies the dorsalmost portion of the anterior precuneus, extending anteriorly just behind the dorsal tip of the cingulate sulcus. hPE (purple) occupies the dorsomedial portion of the post-central gyrus just over the tip of the cingulate sulcus. Other details about the individual variability of the location of hPEc and hPE are provided in the previous paragraph on the somatomotor task and in Table 1.

3.2.6. *Resting-state connectivity of functionally defined hPEc and neighboring regions V6Ad and hPE*

We examined the pattern of cortical connections associated with hPEc and neighbouring regions (V6Ad and hPE) aiming at verifying that hPEc (1) showed the same pattern of cortico-cortical connections observed in the monkey PEc, thus supporting the proposed homology, and (2) belonged to a cortical network partially segregated from that of V6Ad and hPE, thus confirming that it is functionally-distinct from the neighboring areas.

The whole-brain pattern connectivity of the region hPEc (Fig. 9A; see also Supplementary Table 4 for details) was very similar to the pattern of cortico-cortical connections observed in the monkey PEc after neural tracer injections (Bakola et al., 2010, Fig. 9B for a direct comparison). Specifically, in both species PEc connections included regions in:

1) Lateral parietal cortex. The functional connectivity of hPEc extends into insular and parieto-temporal cortices, where there are vestibular and proprioceptive regions as PIC, PIVC (Frank et al., 2016) and the secondary somatosensory area (S-II) as well, which has a rough somatotopic organization (Eickhoff et al., 2006; Ruben et al., 2001; for macaque, see Fig. 9B: PIVC, PGop, PG). hPEc is also connected laterally with multisensory regions into the SPL located behind and along the postcentral sulcus (Fig. 9B: MIP, dMIP), including few portions of the somatosensory BA3b and BA3a regions (Fig. 9B: area 2) and with regions anterior to it. The large lateral cluster in the SPL likely overlaps the parietal homunculus found by Huang et al. (2012), that represents the entire body extending on the whole extent of the postcentral sulcus.
2) Frontal cortex. As in macaque (Fig. 9B: F2, F3), hPEc also showed fronto-medial connections with Brodmann area 6, where in human the supplementary motor region (SMA) classically considered to be somatotopically organized (Amiez and Petrides, 2014) is located. Laterally, hPEc connections spread to dorsal frontal areas at the junction between the superior frontal sulcus (SFS) and precentral sulcus (pCS), a region likely homologue to monkey area F2 (Matelli et al., 1991), where a premotor region responding to hand-reaching movements has been found (Tosoni et al., 2008; Amiez et al., 2006). Monkey tracing studies found that PEc has robust connection

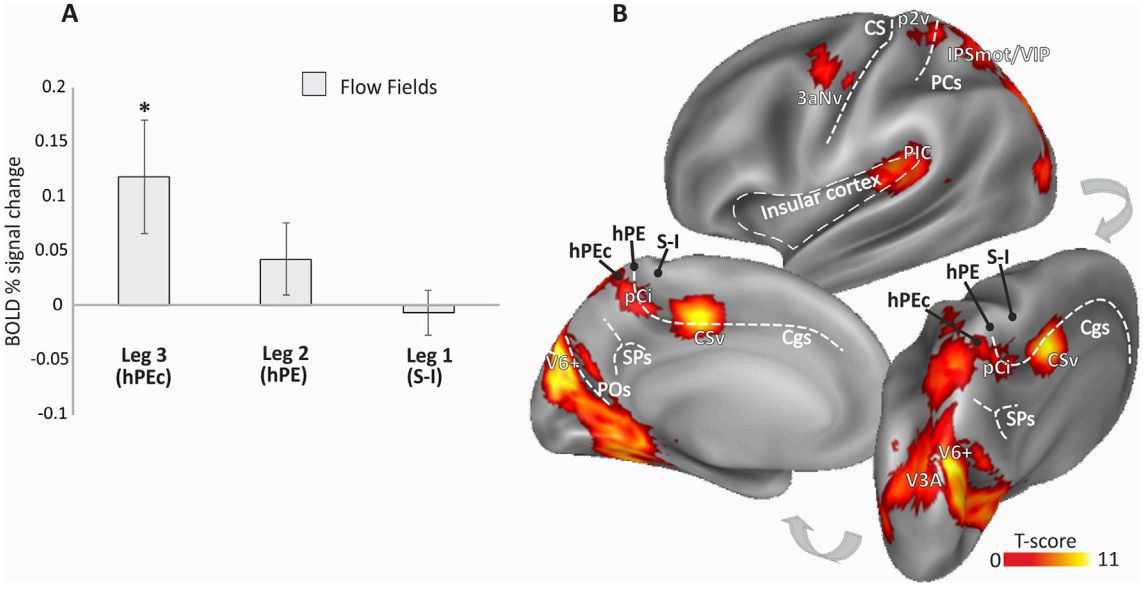

Fig. 7. Visual task: visual motion related responses within the three leg-related regions. (A) Plots for each region indicates the averaged BOLD percent signal change ± standard error of the mean across subjects for Flow Field blocks (relative to random motion). Asterisks refer to T-test versus zero. *p = 0.02. **(B)** Group activation maps overlaid onto atlas Conte69 and rendered in three different inflated views (medial, lateral and dorsomedial). The centers of mass of hPEc, hPE and S-I are marked by a black spot. Areas more active during the coherent motion are labelled: PIC (Parieto Insular Cortex), IPSmot/VIP, intraparietal motion area/ventral intraparietal, V6+, pCi (posterior Cingulate area), CSv (Cingulate Sulcus Visual Area), V3A. Other labels and logos are as in Figs. 3 and 5.

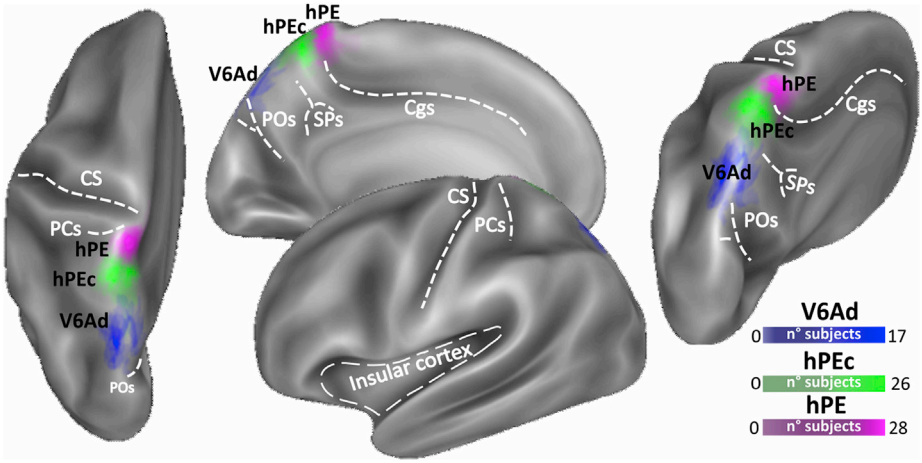

Fig. 8. Brain location of hPEc and its neighboring regions. Individual ROIs are overlapped onto Conte69 brain atlas in different views (superior, medial, lateral, and dorsomedial) to form group-probabilistic ROIs. The color scale indicates the proportion of subjects whose ROI included that surface node, thus the probability that the node is included in the ROI. Color indicates regions: V6Ad, blue; hPEc, green; hPE, purple. V6Ad was identified using the visuomotor task as described in Tosoni et al. (2015), (see Methods for details). Other labels and symbols are as in previous Figures.

with F2, where the precentral dimple marks the approximate border between lateral arm representation and medial leg representation (Bakola et al., 2010).

3) Mesial cortex. hPEc was functionally connected medially with a large territory that included the posterior precuneus (in correspondence with the anterior portion of hV6Ad), the cortical territory into and above the tip of the ramus marginalis of the cingulate sulcus (Fig. 9B: PE, PEci), where we have identified hPE, and anterior motor regions in the cingulate sulcus (Fig. 9A: 31a, 23c, p24pr, 24d, a24pr; Fig. 9B: 31, 23, 24d). Notably, the connectivity map included only the most dorsomedial portion of the primary somatosensory (Fig. 9A: BA3a; Fig. 9B: area 2) and motor cortices (Fig. 9A: BA4a; Fig. 9B: F1) where lower limb representations have been found (Akselrod et al., 2017; Tal et al., 2017; Di Russo et al., 2006).

Overall, the great similarity in the whole-brain pattern connectivity of PEc across the two species further supports the view of a homology between human and macaque area PEc.

Fig. 10 shows the results of the formal direct comparison among the fcMRI maps associated with V6Ad, hPEc and hPE regions (see also Supplementary Table 5 for details). Taken together, these connectivity maps depict partially segregated patterns of cortical connections:

1) As shown in Fig. 10A, V6Ad is more connected than hPEc and hPE (blue and green, respectively) with posterior regions like the POs (where area V6 is located) and with the precuneate cortex, spreading to lateral parietal attentional regions into the IPS and the ventrolateral prefrontal cortex (BA46). Compared to hPE, the cortical connections of V6Ad (Fig. 10A, green) spread over the ventrolateral frontal areas into the inferior frontal sulcus.
2) hPEc compared to hPE and V6Ad (Fig. 10B, green and red, respectively) showed more connectivity with the posterior precuneate cortex (where V6Ad is located) and with insular (laterally) and motor cingulate (medially) cortex, where connections of hPEc spread more anteriorly. hPEc and hPE, compared to V6Ad (Fig. 10B and C, red), showed stronger functional connectivity with primary motor areas

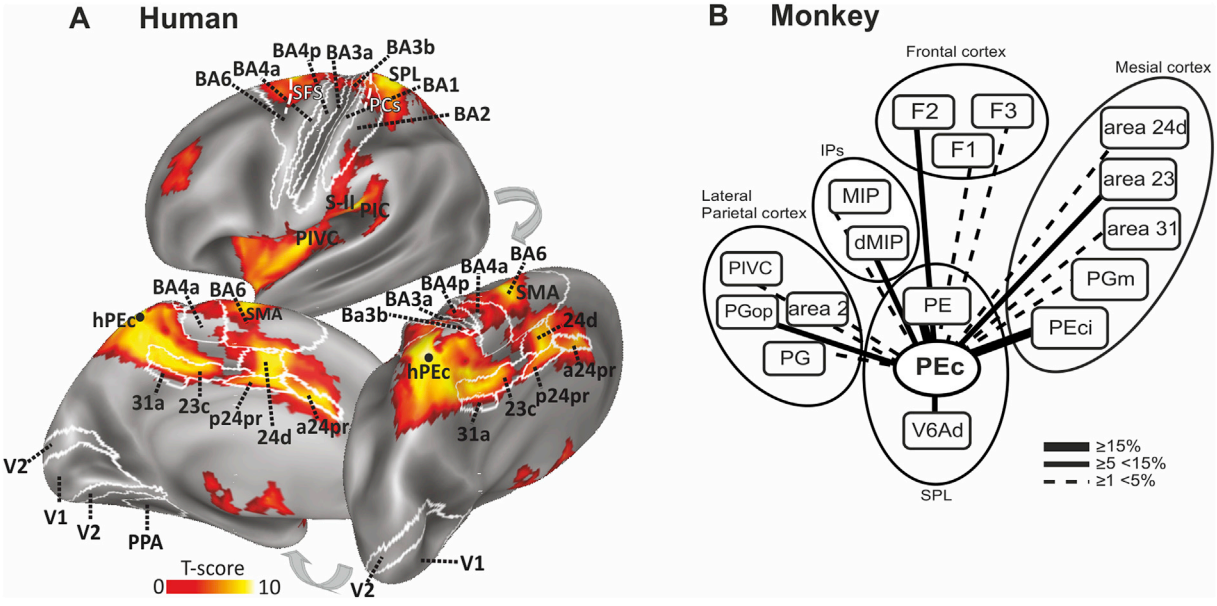

Fig. 9. The pattern of connectivity of PEc region. (A) Whole-brain connectivity map associated to the functionally defined hPEc region is superimposed over the Conte69 atlas (Van Essen et al., 2011). Inflated representation of the left hemisphere shown in lateral, medial and dorsomedial views. The borders of previously identified areas (Brodmann, 1909; Van Essen et al., 2011; Sulpizio et al., 2013; Glasser et al., 2016) are indicated using solid white lines. The color scale in B indicates the statistical significance of the activations using the FDR corrected p-values. **(B)** Flow chart of the significant projections to area PE (modified from Bakola et al., 2013).

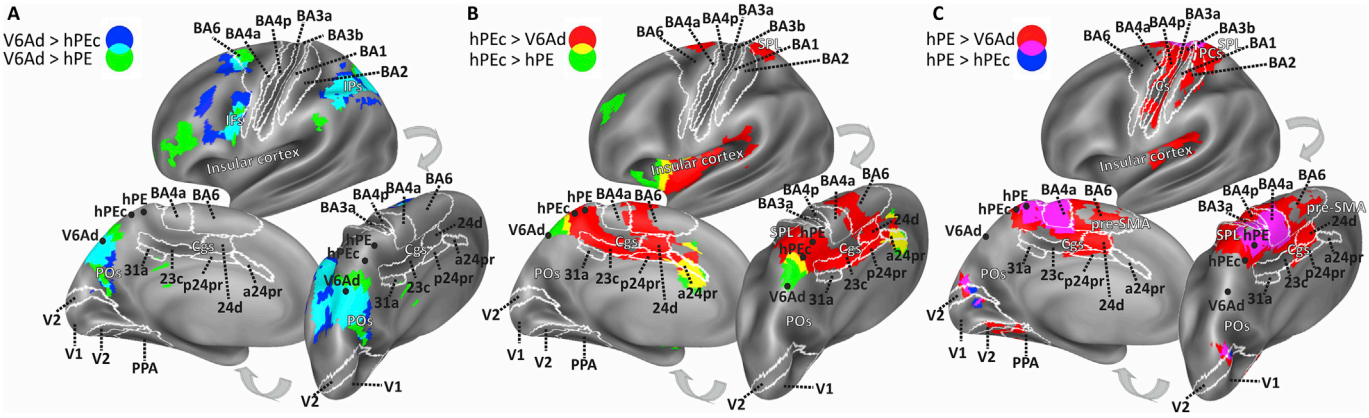

Fig. 10. Functional segregation of pattern connectivity associated with V6Ad, hPEc and hPE. (A) Regions showing stronger functional connectivity with V6Ad than with hPEc (blue), hPE (green) or both (cyan). **(B)** Regions showing stronger functional connectivity with hPEc than with V6Ad (red), hPE (green) or both (yellow). **(C)** Regions showing stronger functional connectivity with hPE than V6Ad (red), hPEc (blue) or both (magenta). The borders of previously identified areas (Brodmann, 1909; Van Essen et al., 2011; Sulpizio et al., 2013; Glasser et al., 2016) are indicated using solid white lines. Other labels are as in Fig. 9A.

and cingulate motor areas, medially, and with vestibular and insular cortices as well as the somatosensory portion of the SPL, laterally.

3) hPE, compared to both V6Ad and hPEc (Fig. 10C, red and blue, respectively), was much widely connected with sensory and motor medial and lateral (BA3 and BA4) regions into the Central sulcus (CS) and the dorsal SPL around the postcentral sulcus (Fig. 10C, purple). Medially, hPE showed dense connections also with portion of the middle cingulate gyrus and part of the BA6 (Fig. 10C, red), where the pre-SMA area is presumably located. In human, but not in monkey, the connectivity of hPE extends into peripheral representations of occipital early visual areas (V1/V2), and more anteriorly into the lingual-parahippocampal gyrus, where it overlaps with the probabilistic scene-responsive PPA region (Sulpizio et al., 2013).

Overall, this analysis highlighted that the visuomotor V6Ad and the somatosensory regions hPEc and hPE belonged to partially separate networks. hPEc is more connected than neighboring V6Ad and hPE to vestibular regions, visuomotor precuneate cortex and sensorimotor regions of the cingulate sulcus, representing an intermediate functional and anatomical region between V6Ad and hPE. It is worth noting that the differences in the pattern of connections observed between these three regions is strikingly similar to that observed in previous macaque studies using neural tracer injections (Gamberini et al., 2009; Bakola et al., 2010, 2013).

4. Discussion

Here we used combined fMRI techniques (i.e., individual mapping, task-evoked paradigms and resting-state functional connectivity) to study the lower limb representation in the human dorsomedial parietal cortex in the attempt to define the human homologue of macaque area PEc.

By looking at multiple leg representations in the human dorsomedial parietal cortex, we successfully identified a medial parietal region (hPEc) in a large sample of subjects. hPEc was located in the most anterior part of the dorsal precuneate cortex, anterior to the subparietal sulcus and posterior to the ascending ramus of the cingulate sulcus. Consistent with macaque evidence, hPEc is located anteriorly to area hV6Ad and posteriorly to area hPE. Present data reveal that hPEc, like macaque PEc, is an association area containing somatomotor, visuomotor, and visual responses, strengthening the case for the homology between these cortical areas in humans and macaques.

In agreement with previous macaque studies (Breveglieri et al., 2006; 2008; Gamberini et al., 2018), we found that the hPEc responds to either upper and lower limb movements during the somatomotor task. Its functional profile is different from that observed in the two anterior somatosensory regions, hPE and S-I. Those areas respond only to leg movements, as expected based on their somatotopic organization. Further, in both human and monkey the response to leg movements involves a strip of cortex extending from the dorsal precuneate cortex to the medial sensorimotor/motor cortex representing the lower limb. Thus, for both species, the PEc is the first region along the posterior-to-anterior axis that responds to leg movements, further strengthening the case for the homology.

Beyond somatosensory properties, the macaque PEc also shows visuomotor responses. For instance, monkey studies using visually guided reaching tasks in both 2D and 3D space (Battaglia-Mayer et al., 2001; Ferraina et al., 2001; Hadjidimitrakis et al., 2015; Piserchia et al., 2017) have shown reach-related neural activity in the macaque PEc. In line with these findings, we found that also the human PEc shows great activation in the visuomotor task implying delayed hand/foot pointing movements towards a visual target (see Fig. 6). Similarly to the two anterior leg-related regions hPE and S-I, hPEc showed a very strong response during foot-pointing movements but, differently from them, it had a unique functional profile during hand-pointing movements, being the only region among the three showing a positive and reliable response. The hPEc is activated by the pointing action regardless of the effector used. Therefore, the hPEc responsiveness to spatially-directed hand and foot reaching movements, beyond confirming the presence of reaching neurons as in the monkey PEc (Battaglia-Mayer et al., 2001; Ferraina et al., 2001; Hadjidimitrakis et al., 2014, 2015; Piserchia et al., 2017), also supports the lack in this area of a somatotopic organization, as previously observed in macaque (Breveglieri et al., 2006; Gamberini et al., 2018).

In hPEc we observed a negative response to saccadic eye movements. In the macaque literature, evidence on the involvement of the PEc region in eye movements is not fully established. Raffi et al. (2008) investigated the sensitivity of PEc neurons to saccades and eye position and found that the majority of neurons showed pre-saccadic activity and that 26% of neurons show an inhibitory profile during the pre-saccadic period. Other authors found that the activity of most cells in area PEc was influenced by eye position and only a few cells displayed a relationship to saccadic eye movements (Battaglia-Mayer et al., 2001; Ferraina et al., 2001). The relationship between the present results and those reported on monkeys is limited by the fact that we did not separate pre-versus post-saccadic activity, and that we did not test different eye positions to evaluate a sort of 'gain field' effect, as done in a previous fMRI study (Strappini et al., 2015). On the other hand, it is worth noting that only for the eye condition, we observed in hPEc a statistically significant negative response, which could somehow mirror the response inhibition found in macaque.

In the visual domain, it has been reported that macaque PEc hosts visual cells responding not only to moving light/dark bars (Battaglia--Mayer et al., 2001; Ferraina et al., 2001; Squatrito et al., 2001; Breveglieri et al., 2008), but also to optic flow stimuli (Battaglia-Mayer et al., 2001; Raffi et al., 2002, 2010, 2011, 2014). In line with these monkey data, we observed that the hPEc shows a strong response to flow fields (see Fig. 7), while visual sensitivity progressively decreases anterior to hPE and S-I areas. hPE shows a significant but statistically uncorrected response to flow fields, while S-I did not show any significant response at all, in good agreement with the fact that we are moving from visual to somatic regions of the brain.

Lastly, we found that hPEc has functional connections with a broad network of regions belonging to visual, somatosensory, motor, and vestibular system. Taken as a whole, this functional connectivity network includes both regions encoding sensory input in relation to spatial limb positions and areas directly involved in the motor execution. The connectivity of hPEc with both medial somatomotor regions and premotor cortices, all representing the lower limbs, is a relevant result of the current study, and strictly parallels what is observed in the macaque brain (Bakola et al., 2010). Also, the paucity of connections with the inferior premotor cortex, and with low-level sensorimotor areas, unlike the neighboring area PE (Bakola et al., 2013), further supports the homology with monkey PEc.

Overall, functional data on both species conclude in favor of area PEc as a cortical region representing both upper and lower limbs, thus suggesting that it might have a role in controlling and coordinating limb movements during motor actions requiring only leg (e.g., stepping) or both leg and arm (e.g., climbing). Given the sensitivity to visual stimulations, and in particular to optic flow, and the main representation of the lower visual field, PEc could be mostly involved in the control of locomotion (Breveglieri et al., 2008; Bakola et al., 2010; Raffi et al., 2014; Hadjidimitrakis et al., 2015; Gamberini et al., 2018).

4.1. Activations of dorsomedial parietal cortex for hand and foot movements: comparison with previous human studies

While there are no previous detailed studies revealing the human homologue of macaque PEc, many neuroimaging studies have reported hand pointing, reaching, and grasping-related activations extending through the dorsomedial parietal cortex from the POs to the cingulate sulcus (Astafiev et al., 2003; Fernandez-Ruiz et al., 2007; Hagler et al., 2007; Beurze et al., 2007; Tosoni et al., 2008; Filimon et al., 2009; Galati et al., 2011). While some previous studies have reported one large medial parietal region of activation (human parietal reach region, hPRR: Connolly et al., 2003), other studies have reported two distinct activation foci, for pointing and reaching movements, in the medial PPC: one posterior, in the vicinity of the POs, and another anterior, in the anterior precuneus (PO and preCUN: Beurze et al., 2007; POS and aPCU: Filimon et al., 2009; pPRR and aPRR: Tosoni et al., 2008; MP and MD: Galati et al., 2011). Still other studies have reported only an anterior (Astafiev et al., 2003; Fernandez-Ruiz et al., 2007; Hagler et al., 2007) or only a posterior (Beurze et al., 2009; Cavina-Pratesi et al., 2010) activation. A comparison in terms of anatomical position between the present results and the two distinct pointing-responsive foci described above suggests that human areas V6Ad and hPEc correspond quite well to the posterior and anterior reaching regions described in the other studies (see citations above).

Although the medial parietal cortex has been investigated mainly using hand reaching and pointing tasks, several neuroimaging studies have also investigated the cortical representation of the lower limbs, an issue more strictly related to the present study. Some fMRI studies (Heed et al., 2011, 2016; Leoné et al., 2014) have compared hand pointing, foot pointing, and saccade during a delayed movement task to study the effector selectivity of the SPL. They found a region in the anterior precuneus (aPCu), representing both upper and lower limbs and with a higher BOLD response for foot than hand movements. Using repetition suppression paradigm, Heed et al. (2016) revealed limb-specific adaptation effects in the aPCu, isolating a hand-specific cortical portion extending from the postcentral sulcus into the SPL, and a foot-specific portion extending medially to it. Although comparisons between our results and those studies are limited by differences in the methodological approach, as we combined single-mapping with regional analysis while they used group analysis, Medendorp's findings about a foot-specific region in the medial aPCu offers strong support to present delineation of hPEc. Abdollahi et al. (2013) have recently found that a region in the human dorsal SPL, which likely includes the human PEc as defined here, is activated when observing foot actions (e.g. locomotion) and, even more, when observing foot and arm actions (e.g. climbing). This supports a possible role of the human PEc in coordinating limbs for body movements in order to interact with objects while moving, as hypothesized for the monkey PEc (Breveglieri et al., 2008; Bakola et al., 2010; Raffi et al., 2010, 2014; Hadjidimitrakis et al., 2015; Gamberini et al., 2018; Impieri et al., 2018). Future studies are needed to assess whether PEc has differential features during reaching or grasping tasks with respect to other visuomotor areas, as V6Ad. Evidence for a central role of PEc in reaching comes also from neurological studies. It has been reported that a patient with damage of the posterior part of the SPL that likely included the putative human area PEc showed severe impairment of body interaction with the surrounding objects (Kase et al., 1977). Moreover, it has been found that lesions to medial parietal sites impair not only hand-reaching behaviors but also foot-reaching movements (Evans et al., 2013). Overall, neuroimaging and lesion studies in humans support the involvement of the anterior dorsal precuneus (putatively the human PEc) in controlling hand and foot movements, as well as the homology between the caudal SPL of human and non-human primates.

Lastly, a note on the different approach used here with respect to the previous fMRI studies mentioned above. The use of long-range limb movements has so far received little attention in the neuroimaging field, perhaps for the intrinsic difficulty in studying such a type of movement in the MR scanner. The few fMRI studies on this topic preferred presentation of videos showing human actions (e.g., locomotion and climbing), or visuomotor tasks with short-range movements like hand-or foot-pointing under visual guidance. Using this visual-based approach, other authors (e.g., Tosoni et al., 2008; Filimon et al., 2007, 2009; Cavina-Pratesi et al., 2010; Vesia et al., 2010; Heed et al., 2011, 2016; Leoné et al., 2014; Magri et al., 2019) have reported robust upper precuneate activations, extending into the posterior cingulate sulcus, in response to hand or foot movements. Also, other papers from our lab (Galati et al., 2011; Tosoni et al., 2015) reported a hand-pointing-related functional activation in visuomotor tasks spanning from the parieto-occipital sulcus to the most dorsal precuneate cortex. For all these mentioned fMRI studies, the spread of the fMRI activations all over the parietal cortex (which vigorously responds to the presence of a lateralized visual target) has been a drawback for finding separate and effector-selective parietal regions. Here, we instead used a somatomotor task (not contaminated by the presence of visual stimuli or lateralized cues) and we asked our subjects to move limbs in the scanner so to perform real and long-range arm and leg movements without any visuomotor interaction. This approach has been suggested by monkey data, where proprioception and tactile stimulations of arm but not leg in V6A, and arm and leg in PEc activate the areas. The most interesting aspect of this approach is that the whole PPC is silent with the only exception of the most anterior dorsal precuneus which respond during arm and leg movements. Thus, somatic and tactile representations are stronger in hPEc than hV6A, like in macaque. Thanks to the lack of arm-related activation in the posterior precuneate cortex and POs, we were able to isolate a tactile-motor region with functional and connectivity properties very similar to those observed in the macaque PEc. Note that we also used a visuomotor task, and in that case we found comparable results with respect to previously mentioned fMRI studies (that is, a great spread of activation on the PPC). The different response observed in the PPC in the two tasks further supports the role of the PPC in visuomotor integration and suggest that using a somatomotor

task without visual guidance of the movement is not ideal to activate the PPC, but is an effective expedient to isolate effector-related responses in somatomotor cortical regions, like hPEc and hPE.

4.2. Functional responses in other areas of the dorsomedial parietal lobe

Anterior to PEc, positive BOLD responses to leg movements were detected also in areas hPE and S-I. In these two regions, we found only foot-related activation in both the somatomotor and visuomotor task, as expected based on the somatotopic organization of PE (Taoka et al., 1998, 2000; Padberg et al., 2007, Seelke et al., 2012) and S-I (Di Russo et al., 2006; Golaszewski et al., 2006; Huang et al., 2012; Akselrod et al., 2017; Huang and Sereno, 2018). In addition, during the arm movements we also found negative responses in the portion of S-I defined here (i.e., using leg movements), a result in line with a recent study by Tal et al. (2017) who found positive BOLD responses in contralateral S-I after unilateral stimulations of different body parts, but also negative responses in regions of S-I not representing the stimulated parts of the body.

Huang et al. (2012) reported that in the anterior SPL territory there is a rough somatotopic representation of the entire body, a high-level parietal homunculus they called parietal body area (PBA). Initial evidence suggested that this multisensory homunculus contains multiple aligned visual-tactile representations. The medial most part of this homunculus, representing the lower limbs, was found at the level of the postcentral sulcus, just behind the primary somatosensory cortex, in a cortical region likely corresponding to our human PE. Our results in the visual motion task support this hypothesis. Indeed, the marginally significant visual motion response found in hPE is in line with the only partial overlap between visual and tactile maps found by Huang et al. (2012) in correspondence of the lower limb representation of area PBA. Overall, the presence of the PBA found by Huang et al. (2012) supports our vision of a further cortical leg representation in between S-I and hPEc.

5. Conclusions

We revealed the existence in the dorsal precuneate cortex of a region with functional and connectivity properties very similar to those observed in the macaque PEc. This region responds to arm and leg movements and is part of a sensorimotor dorsomedial network showing strong connections with both the visuomotor area V6Ad, involved in the control of reach-to-grasp movements, and with motor and premotor areas representing lower limbs. Based on similarity in brain position, relationships with the neighboring areas, functional organization and cortical connections, we propose that the precuneate cortical region is the human homologue of macaque area PEc. Our study extends the inventory of the high order association areas in the human posterior parietal cortex and opens up the way to the study of the neural basis of locomotion testing regions of the parietal cortex responding to both flow fields and active leg movements (like the hPEc; see also Serra et al., 2019). In addition, using a somatomotor task we found that the whole posterior parietal cortex behind PEc was surprisingly silent (as never seen in the past using visuomotor tasks). Our approach therefore provides a valuable way to segregate the ‘visual’ from the ‘somatomotor’ responses in the parietal cortex. This approach has been suggested by monkey data (where proprioception and tactile stimulations of arm and leg segregate sub-regions from the POs to the dorsal precuneus) and this strengthens the importance of looking for homologies, especially when, as in this case, the possible homology with the monkey brain guided us in the study of the organization of the human SPL.

Conflicts of interest

We have no conflict of interest to declare.

Acknowledgments

The work was supported by the University of Foro Italico (grant number FFABR) to Sabrina Pitzalis. We thank M. Gamberini for helping with figures.

Appendix A. Supplementary data

Supplementary data to this article can be found online at https://doi.org/10.1016/j.neuroimage.2019.116092.

References

Abdollahi, R.O., Jastorff, J., Orban, G.A., 2013. Common and segregated processing of observed actions in human SPL. Cerebr. Cortex 23, 2734–2753.
Akselrod, M., Martuzzi, R., Serino, A., van der Zwaag, W., Gassert, R., Blanke, O., 2017. Anatomical and functional properties of the foot and leg representation in areas 3b, 1 and 2 of primary somatosensory cortex in humans: a 7 T fMRI study. Neuroimage 159, 473–487.
Amiez, C., Kostopoulos, P., Champod, A., Petrides, M., 2006. Local morphology predicts functional organization of the dorsal premotor region in the human brain. J. Neurosci. 26, 2724–2731.
Amiez, C., Petrides, M., 2014. Neuroimaging evidence of the anatomo-functional organization of the human cingulate motor areas. Cerebr. Cortex 24, 563–578.
Astafiev, S.V., Shulman, G.L., Stanley, C.M., Snyder, A.Z., Van Essen, D.C., Corbetta, M., 2003. Functional organization of human intraparietal and frontal cortex for attending, looking, and pointing. J. Neurosci. 23, 4689–4699.
Bakola, S., Gamberini, M., Passarelli, L., Fattori, P., Galletti, C., 2010. Cortical connections of parietal field PEc in the macaque: linking vision and sensation for the control of limb action. Cerebr. Cortex 20, 2592–2604.
Bakola, S., Passarelli, L., Gamberini, M., Fattori, P., Galletti, C., 2013. Cortical connectivity suggests a role in limb coordination for macaque area PE of the superior parietal cortex. J. Neurosci. 33, 6648–6658.
Battaglia-Mayer, A., Ferraina, S., Genovesio, A., et al., 2001. Eye-hand coordination during reaching. II. An analysis of the relationships between visuomanual signals in parietal cortex and parieto-frontal association projections. Cerebr. Cortex 11, 528–544.
Behzadi, Y., Restom, K., Liau, J., Liu, T.T., 2007. A component based noise correction method (CompCor) for BOLD and perfusion based fMRI. Neuroimage 37, 90–101.
Besle, J., Sanchez-Panchuelo, R.-M., Bowtell, R., Francis, S., Schluppeck, D., 2013. Single-subject fMRI mapping at 7 T of the representation of fingertips in S1: a comparison of event-related and phase-encoding designs. J. Neurophysiol. 109, 2293–2305.
Beurze, S.M., de Lange, F.P., Toni, I., Medendorp, W.P., 2007. Integration of target and effector information in the human brain during reach planning. J. Neurophysiol. 97, 188–199.
Beurze, S.M., de Lange, F.P., Toni, I., Medendorp, W.P., 2009. Spatial and effector processing in the human parietofrontal network for reaches and saccades. J. Neurophysiol. 101, 3053–3062.
Breveglieri, R., Galletti, C., Gamberini, M., Passarelli, L., Patrizia, F., 2006. Somatosensory cells in area PEc of macaque posterior parietal cortex. J. Neurosci. 26, 3679–3684.
Breveglieri, R., Galletti, C., Monaco, S., Fattori, P., 2008. Visual, somatosensory, and bimodal activities in the macaque parietal area PEc. Cerebr. Cortex 18, 806–816.
Brodmann, K., 1909. Vergleichende Lokalisationslehre der Grosshirnrinde. Barth, Leipzig (Reprinted 1925).
Cardin, V., Smith, A.T., 2010. Sensitivity of human visual and vestibular cortical regions to egomotion-compatible visual stimulation. Cerebr. Cortex 20, 1964–1973.
Cavina-Pratesi, C., Monaco, S., Fattori, P., Galletti, C., McAdam, T.D., Quinlan, D.J., Goodale, M.A., Culham, J.C., 2010. Functional magnetic resonance imaging reveals the neural substrates of arm transport and grip formation in reach-to-grasp actions in humans. J. Neurosci. 30, 10306–10323.
Chumbley, J., Worsley, K., Flandin, G., Friston, K., 2010. Topological FDR for neuroimaging. Neuroimage 49, 3057–3064.
Connolly, J.D., Andersen, R.A., Goodale, M.A., 2003. FMRI evidence for a “parietal reach region” in the human brain. Exp. Brain Res. 153, 140–145.
Crossland, M.D., Morland, A.B., Feely, M.P., Von Dem Hagen, E., Rubin, G.S., 2008. The effect of age and fixation instability on retinotopic mapping of primary visual cortex. Investig. Ophthalmol. Vis. Sci. 49, 3734–3739.
Dale, A.M., Fischl, B., Sereno, M.I., 1999. Cortical surface-based analysis: I. Segmentation and surface reconstruction. Neuroimage 9, 179–194.
Desikan, R.S., Ségonne, F., Fischl, B., Quinn, B.T., Dickerson, B.C., Blacker, D., Buckner, R.L., Dale, A.M., Maguire, R.P., Hyman, B.T., 2006. An automated labeling system for subdividing the human cerebral cortex on MRI scans into gyral based regions of interest. Neuroimage 31, 968–980.
Di Russo, F., Committeri, G., Pitzalis, S., Spitoni, G., Piccardi, L., Galati, G., Catagni, M., Nico, D., Guariglia, C., Pizzamiglio, L., 2006. Cortical plasticity following surgical extension of lower limbs. Neuroimage 30, 172–183.
Di Russo, F., Pitzalis, S., Spinelli, D., 2003. Fixation stability and saccadic latency in élite shooters. Vis. Res. 43, 1837–1845.
Economo, C. von, Koskinas, G.N., 1925. Die Cytoarchitektonik der Hirnrinde des erwachsenen Menschen. Springer Verlag, Vienna (Textband und Atlas).

Eickhoff, S.B., Amunts, K., Mohlberg, H., Zilles, K., 2006. The human parietal operculum. II. Stereotaxic maps and correlation with functional imaging results. Cerebr. Cortex 16, 268–279.
Epstein, R.A., 2008. Parahippocampal and retrosplenial contributions to human spatial navigation. Trends Cogn. Sci. 12 (10), 388–396.
Epstein, R.A., Kanwisher, N., 1998. A cortical representation of the local visual environment. Nature 392, 598–601.
Evans, C., Milner, A.D., Humphreys, G.W., Cavina-Pratesi, C., 2013. Optic ataxia affects the lower limbs: evidence from a single case study. Cortex 49, 1229–1240.
Fattori, P., Breveglieri, R., Marzocchi, N., Filippini, D., Bosco, A., Galletti, C., 2009. Hand orientation during reach-to-grasp movements modulates neuronal activity in the medial posterior parietal area V6A. J. Neurosci. 29, 1928–1936.
Fattori, P., Kutz, D.F., Breveglieri, R., Marzocchi, N., Galletti, C., 2005. Spatial tuning of reaching activity in the medial parieto-occipital cortex (area V6A) of macaque monkey. Eur. J. Neurosci. 22, 956–972.
Fattori, P., Raos, V., Breveglieri, R., Bosco, A., Marzocchi, N., Galletti, C., 2010. The dorsomedial pathway is not just for reaching: grasping neurons in the medial parieto-occipital cortex of the macaque monkey. J. Neurosci. 30, 342–349.
Fernandez-Ruiz, J., Goltz, H.C., DeSouza, J.F.X., Vilis, T., Crawford, J.D., 2007. Human parietal "reach region" primarily encodes intrinsic visual direction, not extrinsic movement direction, in a visual-motor dissociation task. Cerebr. Cortex 17, 2283–2292.
Ferraina, S., Battaglia-Mayer, A., Genovesio, A., Marconi, B., Onorati, P., Caminiti, R., 2001. Early coding of visuomanual coordination during reaching in parietal area PEc. J. Neurophysiol. 85, 462–467.
Filimon, F., Nelson, J.D., Hagler, D.J., Sereno, M.I., 2007. Human cortical representations for reaching: mirror neurons for execution, observation, and imagery. Neuroimage 37, 1315–1328.
Filimon, F., Nelson, J.D., Huang, R.-S., Sereno, M.I., 2009. Multiple parietal reach regions in humans: cortical representations for visual and proprioceptive feedback during on-line reaching. J. Neurosci. 29, 2961–2971.
Fischer, E., Bülthoff, H.H., Logothetis, N.K., Bartels, A., 2012. Human areas V3A and V6 compensate for self-induced planar visual motion. Neuron 73, 1228–1240.
Fox, M.D., Raichle, M.E., 2007. Spontaneous fluctuations in brain activity observed with functional magnetic resonance imaging. Nat. Rev. Neurosci. 8, 700–711.
Frank, S.M., Baumann, O., Mattingley, J.B., Greenlee, M.W., 2014. Vestibular and visual responses in human posterior insular cortex. J. Neurophysiol. 112, 2481–2491.
Frank, S.M., Wirth, A.M., Greenlee, M.W., 2016. Visual-vestibular processing in the human Sylvian fissure. J. Neurophysiol. 116, 263–271.
Galati, G., Committeri, G., Pitzalis, S., Pelle, G., Patria, F., Fattori, P., Galletti, C., 2011. Intentional signals during saccadic and reaching delays in the human posterior parietal cortex. Eur. J. Neurosci. 34, 1871–1885.
Galati, G., Committeri, G., Spitoni, G., Aprile, T., Di Russo, F., Pitzalis, S., Pizzamiglio, L., 2008. A selective representation of the meaning of actions in the auditory mirror system. Neuroimage 40, 1274–1286.
Galletti, C., Fattori, P., Battaglini, P.P., Shipp, S., Zeki, S., 1996. Functional demarcation of a border between areas V6 and V6A in the superior parietal gyrus of the macaque monkey. Eur. J. Neurosci. 8, 30–52.
Galletti, C., Fattori, P., Gamberini, M., Kutz, D.F., 1999a. The cortical visual area V6: brain location and visual topography. Eur. J. Neurosci. 11, 3922–3936.
Galletti, C., Fattori, P., Kutz, D.F., Gamberini, M., 1999b. Brain location and visual topography of cortical area V6A in the macaque monkey. Eur. J. Neurosci. 11, 575–582.
Gamberini, M., Dal Bò, G., Breveglieri, R., Briganti, S., Passarelli, L., Fattori, P., Galletti, C., 2018. Sensory properties of the caudal aspect of the macaque's superior parietal lobule. Brain Struct. Funct. 223, 1863–1879.
Gamberini, M., Galletti, C., Bosco, A., Breveglieri, R., Fattori, P., 2011. Is the medial posterior parietal area V6A a single functional area? J. Neurosci. 31, 5145–5157.
Gamberini, M., Passarelli, L., Fattori, P., et al., 2009. Cortical connections of the visuomotor parietooccipital area V6Ad of the macaque monkey. J. Comp. Neurol. 513, 622–642.
Glasser, M.F., Coalson, T.S., Robinson, E.C., Hacker, C.D., Harwell, J., Yacoub, E., Ugurbil, K., Andersson, J., Beckmann, C.F., Jenkinson, M., Smith, S.M., Van Essen, D.C., 2016. A multi-modal parcellation of human cerebral cortex. Nature 536, 171–178.
Glasser, M.F., Sotiropoulos, S.N., Wilson, J.A., Coalson, T.S., Fischl, B., Andersson, J.L., et al., 2013. The minimal preprocessing pipelines for the Human Connectome Project. Neuroimage 80, 105–124.
Golaszewski, S.M., Siedentopf, C.M., Koppelstaetter, F., Fend, M., Ischebeck, A., Gonzalez-Felipe, V., Haala, I., Struhal, W., Mottaghy, F.M., Gallasch, E., Felber, S.R., Gerstenbrand, F., 2006. Human brain structures related to plantar vibrotactile stimulation: a functional magnetic resonance imaging study. Neuroimage 29, 923–929.
Goodale, M.A., Milner, A.D., 1992. Separate visual pathways for perception and action. Trends Neurosci. 15, 20–25.
Guldin, W.O., Grüsser, O.J., 1998. Is there a vestibular cortex? Trends Neurosci. 21, 254–259.
Hadjidimitrakis, K., Bertozzi, F., Breveglieri, R., et al., 2014. Common neural substrate for processing depth and direction signals for reaching in the monkey medial posterior parietal cortex. Cerebr. Cortex 24, 1645–1657.
Hadjidimitrakis, K., Dal, B.G., Breveglieri, R., Galletti, C., Fattori, P., 2015. Overlapping representations for reach depth and direction in caudal superior parietal lobule of macaques. J. Neurophysiol. 114, 2340–2352.
Hagler Jr., D.J., Riecke, L., Sereno, M.I., 2007. Parietal and superior frontal visuospatial maps activated by pointing and saccades. Neuroimage 35, 1562–1577.
Heed, T., Beurze, S.M., Toni, I., Röder, B., Medendorp, W.P., 2011. Functional rather than effector-specific organization of human posterior parietal cortex. J. Neurosci. 31, 3066–3076.
Heed, T., Leone, F.T.M., Toni, I., Medendorp, W.P., 2016. Functional versus effector-specific organization of the human posterior parietal cortex: revisited. J. Neurophysiol. 116, 1885–1899.
Huang, R., Sereno, M.I., 2018. Multisensory and Sensorimotor Maps, first ed. The Parietal Lobe. Elsevier B.V.
Huang, R.S., Chen, C., Tran, A.T., Holstein, K.L., Sereno, M.I., 2012. Mapping multisensory parietal face and body areas in humans. Proc. Natl. Acad. Sci. U.S.A. 109, 18114–18119.
Impieri, D., Gamberini, M., Passarelli, L., Rosa, M.G.P., Galletti, C., 2018. Thalamo-cortical projections to the macaque superior parietal lobule areas PEc and PE. J. Comp. Neurol. 526, 1041–1056.
Kase, C.S., Troncoso, J.F., Court, J.E., Tapia, J.F., Mohr, J.P., 1977. Global spatial disorientation. J. Neurol. Sci. 34, 267–278.
Kwong, K.K., Belliveau, J.W., Chesler, D.A., Goldberg, I.E., Weisskoff, R.M., Poncelet, B.P., Kennedy, D.N., Hoppel, B.E., Cohen, M.S., Turner, R., 1992. Dynamic magnetic resonance imaging of human brain activity during primary sensory stimulation. Proc. Natl. Acad. Sci. U.S.A. 89, 5675–5679.
Leoné, F.T.M., Heed, T., Toni, I., Medendorp, W.P., 2014. Understanding effector selectivity in human posterior parietal cortex by combining information patterns and activation measures. J. Neurosci. 34, 7102–7112.
Levy, I., Schluppeck, D., Heeger, D.J., Glimcher, P.W., 2007. Specificity of human cortical areas for reaches and saccades. J. Neurosci. 27, 4687–4696.
Luppino, G., Ben Hamed, S., Gamberini, M., Matelli, M., Galletti, C., 2005. Occipital (V6) and parietal (V6A) areas in the anterior wall of the parieto-occipital sulcus of the macaque: a cytoarchitectonic study. Eur. J. Neurosci. 21, 3056–3076.
Magri, C., Fabbri, S., Caramazza, A., Lingnau, A., 2019. Directional tuning for eye and arm movements in overlapping regions in human posterior parietal cortex. Neuroimage 191, 234–242.
Mangan, A.P., Whitaker, R.T., 1999. Partitioning 3D surface meshes using watershed segmentation. IEEE Trans. Vis. Comput. Graph. 5 (4), 308–321.
Margulies, D.S., Vincent, J.L., Kelly, C., Lohmann, G., Uddin, L.Q., Biswal, B.B., Villringer, A., Castellanos, F.X., Milham, M.P., Petrides, M., 2009. Precuneus shares intrinsic functional architecture in humans and monkeys. Proc. Natl. Acad. Sci. U.S.A. 106, 20069–20074.
Martuzzi, R., van der Zwaag, W., Farthouat, J., Gruetter, R., Blanke, O., 2014. Human finger somatotopy in areas 3b, 1, and 2: a 7T fMRI study using a natural stimulus. Hum. Brain Mapp. 35, 213–226.
Matelli, M., Luppino, G., Rizzolatti, G., 1991. Architecture of superior and mesial area 6 and the adjacent cingulate cortex in the macaque monkey. J. Comp. Neurol. 311, 445–462.
Nelson, A.J., Chen, R., 2008. Digit somatotopy within cortical areas of the postcentral gyrus in humans. Cerebr. Cortex 18, 2341–2351.
Oldfield, R.C., 1971. The assessment and analysis of handedness: the Edinburgh inventory. Neuropsychologia 9, 97–113.
Padberg, J., Franca, J.G., Cooke, D.F., Soares, J.G.M., Rosa, M.G.P., Fiorani, M., Gattass, R., Krubitzer, L., 2007. Parallel evolution of cortical areas involved in skilled hand use. J. Neurosci. 27, 10106–10115.
Pandya, D.N., Seltzer, B., 1982. Intrinsic connections and architectonics of posterior parietal cortex in the rhesus monkey. J. Comp. Neurol. 204, 196–210.
Piserchia, V., Breveglieri, R., Hadjidimitrakis, K., Bertozzi, F., Galletti, C., Fattori, P., 2017. Mixed body/hand reference frame for reaching in 3D space in macaque parietal area PEc. Cerebr. Cortex 27, 1976–1990.
Pitzalis, S., Bozzacchi, C., Bultrini, A., Fattori, P., Galletti, C., Di Russo, F., 2013a. Parallel motion signals to the medial and lateral motion areas V6 and MT+. Neuroimage 67, 89–100.
Pitzalis, S., Fattori, P., Galletti, C., 2013b. The functional role of the medial motion area V6. Front. Behav. Neurosci. 6, 91.
Pitzalis, S., Fattori, P., Galletti, C., 2015. The human cortical areas V6 and V6A. Vis. Neurosci. 32, E007.
Pitzalis, S., Galletti, C., Huang, R.-S., Patria, F., Committeri, G., Galati, G., Fattori, P., Sereno, M.I., 2006. Wide-field retinotopy defines human cortical visual area V6. J. Neurosci. 26, 7962–7973.
Pitzalis, S., Sdoia, S., Bultrini, A., Committeri, G., Di Russo, F., Fattori, P., Galletti, C., Galati, G., 2013c. Selectivity to translational egomotion in human brain motion areas. PLoS One 8, 1–14.
Pitzalis, S., Sereno, M.I., Committeri, G., Fattori, P., Galati, G., Patria, F., Galletti, C., 2010. Human V6: the medial motion area. Cerebr. Cortex 20, 411–424.
Pitzalis, S., Sereno, M.I., Committeri, G., Fattori, P., Galati, G., Tosoni, A., Galletti, C., 2013d. The human homologue of macaque area V6A. Neuroimage 82, 517–530.
Pitzalis, S., Strappini, F., Bultrini, A., Di Russo, F., 2018. Detailed spatiotemporal brain mapping of chromatic vision combining high-resolution VEP with fMRI and retinotopy. Hum. Brain Mapp. 39, 2868–2886.
Pitzalis, S., Strappini, F., De Gasperis, M., Bultrini, A., Di Russo, F., 2012. Spatiotemporal brain mapping of motion-onset VEPs combined with fMRI and retinotopic maps. PLoS One 7, e35771.
Power, J.D., Barnes, K.A., Snyder, A.Z., Schlaggar, B.L., Petersen, S.E., 2012. Spurious but systematic correlations in functional connectivity MRI networks arise from subject motion. Neuroimage 59 (3), 2142–2154. http://doi.org/10.1016/j.neuroimage.2011.10.018.
Raffi, M., Ballabeni, A., Maioli, M.G., Squatrito, S., 2008. Neuronal responses in macaque area PEc to saccades and eye position. Neuroscience 156 (3), 413–424.
Raffi, M., Carrozzini, C., Maioli, M.G., Squatrito, S., 2010. Multimodal representation of optic flow in area PEc of macaque monkey. Neuroscience 171, 1241–1255.
Raffi, M., Maioli, M.G., Squatrito, S., 2011. Optic flow direction coding in area PEc of the behaving monkey. Neuroscience 194, 136–149.

Raffi, M., Persiani, M., Piras, A., Squatrito, S., 2014. Optic flow neurons in area PEc integrate eye and head position signals. Neurosci. Lett. 568, 23–28.
Raffi, M., Squatrito, S., Maioli, M.G., 2002. Neuronal responses to optic flow in the monkey parietal area PEc. Cerebr. Cortex 12, 639–646.
Ruben, J., Schwiemann, J., Deuchert, M., Meyer, R., Krause, T., Curio, G., Villringer, K., Kurth, R., Villringer, A., 2001. Somatotopic organization of human secondary somatosensory cortex. Cerebr. Cortex 11, 463–473.
Sanchez-Panchuelo, R.M., Besle, J., Beckett, A., Bowtell, R., Schluppeck, D., Francis, S., 2012. Within-digit functional parcellation of Brodmann areas of the human primary somatosensory cortex using functional magnetic resonance imaging at 7 tesla. J. Neurosci. 32, 15815–15822.
Sánchez-Panchuelo, R.M., Besle, J., Mougin, O., Gowland, P., Bowtell, R., Schluppeck, D., Francis, S., 2014. Regional structural differences across functionally parcellated Brodmann areas of human primary somatosensory cortex. Neuroimage 93, 221–230.
Seelke, A.M.H., Padberg, J.J., Disbrow, E., et al., 2012. Topographic maps within Brodmann's area 5 of macaque monkeys. Cerebr. Cortex 22, 1834–1850.
Sereno, M.I., Pitzalis, S., Martinez, A., 2001. Mapping of contralateral space in retinotopic coordinates by a parietal cortical area in humans. Science 294 (5545), 1350–1354.
Serra, C., Galletti, C., Di Marco, S., Fattori, P., Galati, G., Sulpizio, V., Pitzalis, S., 2019. Egomotion-related visual areas respond to active leg movements. Hum. Brain Mapp. 40 (11), 3174–3191.
Siegel, J.S., Power, J.D., Dubis, J.W., Vogel, A.C., Church, J.A., Schlaggar, B.L., Petersen, S.E., 2014. Statistical improvements in functional magnetic resonance imaging analyses produced by censoring high-motion data points. Hum. Brain Mapp. 35 (5), 1981–1996.
Smith, A.T., Wall, M.B., Thilo, K.V., 2012. Vestibular inputs to human motion-sensitive visual cortex. Cerebr. Cortex 22, 1068–1077.
Squatrito, S., Raffi, M., Maioli, M.G., Battaglia-Mayer, A., 2001. Visual motion responses of neurons in the caudal area PE of macaque monkeys. J. Neurosci. 21, RC130.
Strappini, F., Gilboa, E., Pitzalis, S., Kay, K., McAvoy, M., Nehorai, A., Snyder, A.Z., 2016. Adaptive smoothing based on Gaussian processes regression increases the sensitivity and specificity of fMRI data. Hum. Brain Mapp. 38, 1438–1459.
Strappini, F., Pitzalis, S., Snyder, A.Z., McAvoy, M.P., Sereno, M.I., Corbetta, M., Shulman, G.L., 2015. Eye position modulates retinotopic responses in early visual areas: a bias for the straight-ahead direction. Brain Struct. Funct. 220, 2587–2601.
Sulpizio, V., Boccia, M., Guariglia, C., Galati, G., 2018. Neural codes for one's own position and direction in a real-world "vista" environment. Front. Hum. Neurosci. 30 (12), 167.
Sulpizio, V., Committeri, G., Galati, G., 2014. Distributed cognitive maps reflecting real distances between places and views in the human brain. Front. Hum. Neurosci. 8, 716.
Sulpizio, V., Committeri, G., Lambrey, S., Berthoz, A., Galati, G., 2013. Selective role of lingual/parahippocampal gyrus and retrosplenial complex in spatial memory across viewpoint changes relative to the environmental reference frame. Behav. Brain Res. 242, 62–75.
Tal, Z., Geva, R., Amedi, A., 2017. Positive and negative somatotopic BOLD responses in contralateral versus ipsilateral penfield homunculus. Cerebr. Cortex 27, 962–980.
Taoka, M., Toda, T., Iriki, A., Tanaka, M., Iwamura, Y., 2000. Bilateral receptive field neurons in the hindlimb region of the postcentral somatosensory cortex in awake macaque monkeys. Exp. Brain Res. 134 (2), 139–146.
Taoka, M., Toda, T., Iwamura, Y., 1998. Representation of the midline trunk, bilateral arms, and shoulders in the monkey postcentral somatosensory cortex. Exp. Brain Res. 123, 315–322.
Tootell, R.B., Reppas, J.B., Kwong, K.K., Malach, R., Born, R.T., Brady, T.J., Rosen, B.R., Belliveau, J.W., 1995. Functional analysis of human MT and related visual cortical areas using magnetic resonance imaging. J. Neurosci. 15 (4), 3215–3230.
Tosoni, A., Galati, G., Romani, G.L., Corbetta, M., 2008. Sensory-motor mechanisms in human parietal cortex underlie arbitrary visual decisions. Nat. Neurosci. 11, 1446–1453.
Tosoni, A., Pitzalis, S., Committeri, G., Fattori, P., Galletti, C., Galati, G., 2015. Resting-state connectivity and functional specialization in human medial parieto-occipital cortex. Brain Struct. Funct. 220, 3307–3321.
Uddin, L.Q., Supekar, K., Menon, V., 2010. Typical and atypical development of functional human brain networks: insights from resting-state fMRI. Front. Syst. Neurosci. 4, 1–12.
Van Essen, D.C., Glasser, M.F., Dierker, D.L., Harwell, J., Coalson, T., 2011. Parcellations and hemispheric asymmetries of human cerebral cortex analyzed on surface-based atlases. Cerebr. Cortex 22, 2241–2262.
Van Essen, D.C., Glasser, M.F., Dierker, D.L., Harwell, J., Coalson, T., 2012. Parcellations and hemispheric asymmetries of human cerebral cortex analyzed on surface-based atlases. Cerebr. Cortex 22, 2241–2262.
Vesia, M., Prime, S.L., Yan, X., Sergio, L.E., Crawford, J.D., 2010. Specificity of human parietal saccade and reach regions during transcranial magnetic stimulation. J. Neurosci. 30, 13053–13065.